Disruption of endocytosis through chemical inhibition of clathrin heavy chain function

Wim Dejonghe[1,2,13], Isha Sharma[1,2,13], Bram Denoo[3], Steven De Munck[4,5], Haydar Bulut[6], Evelien Mylle[1,2], Mina Vasileva[7], Qing Lu[1,2], Daniel V. Savatin[1,2], Kiril Mishev[1,2], Wim Nerinckx[4,8], An Staes[9], Andrzej Drozdzecki[10,11], Dominique Audenaert[10,11], Annemieke Madder[3], Jiří Friml[7], Daniël Van Damme[1,2], Kris Gevaert[9], Volker Haucke[12], Savvas Savvides[4,5], Johan Winne[3] and Eugenia Russinova[1,2*]

[1]Department of Plant Biotechnology and Bioinformatics, Ghent University, 9052 Ghent, Belgium.

[2]Center for Plant Systems Biology, VIB, 9052 Ghent, Belgium.

[3]Department of Organic and Macromolecular Chemistry, Polymer Chemistry Research Group and Laboratory for Organic Synthesis, Ghent University, 9000 Ghent, Belgium

[4]Laboratory for Protein Biochemistry and Biomolecular Engineering, Department of Biochemistry and Microbiology, Ghent University, 9000 Ghent, Belgium

[5]Center for Inflammation Research, VIB, 9052, Ghent, Belgium;

[6]

[7]Institute of Science and Technology (IST), Klosterneuburg, Austria

[8]Center for Medical Biotechnology, VIB, 9052 Ghent, Belgium

[9]Department of Medical Protein Research, VIB, 9000 Ghent, Belgium Department of Biochemistry, Ghent University, 9000 Ghent, Belgium

[10]VIB Screening Core, 9052 Ghent, Belgium

[11]Expertise Centre for Bioassay Development and Screening (C-BIOS), Ghent University, 9052 Ghent, Belgium;

[12]

[13]These authors contributed equally to this work.

[*]e-mail: eurus@psb.ugent.be

Clathrin-mediated endocytosis (CME) is an essential and highly dynamic process, required for proper responses to the environment and correct functioning of the eukaryotic cell. Although classical genetic strategies have been used to understand CME, its dynamic and vital nature are difficult to approach with such tools. In contrast, small molecules can acutely and reversibly perturb CME, but only a few CME chemical inhibitors have been applied in plants. Here, we identify endosidin9-17 (ES9-17), a nonprotonophoric analog of the previously discovered mitochondrial uncoupler ES9, as a promising molecule. Affinity-based target identification, *in vitro* binding studies and X-ray crystallography revealed that besides being a protonophore, ES9 bound the terminal domain of the clathrin heavy chain (CHC). Cellular thermal shift and drug affinity-responsive target stability assays established that the CHC binding is the mode of action of ES9-17. Hence, we provide a useful bioactive molecule to selectively probe clathrin functions in eukaryotic cells.

Clathrin-mediated endocytosis (CME) is a major route for internalization of plasma membrane proteins and molecules from the extracellular enviroment[1,2], but its dynamic and essential nature makes it difficult to dissect with classical genetics approaches. Chemical inhibitors of endocytosis are an attractive alternative to the current methods for disrupting the protein function. However, despite the extensive structural and biochemical knowledge about CME in eukaryotic cells[3,4], development of chemical tools to interfere with this process is still at a relative early stage. Until now, a few small molecules have been shown to target particularly the CME machinery in mammalian, yeast or plant systems[5]. Some of the commonly used small molecules are Pitstop2 (ref. 6), Dynasore[7] and the Dynasore-based small molecules, named Dyngo[8], that inhibit CME in mammalian systems by targeting the N-terminal domain (nTD) of the clathrin heavy chain (CHC)[6] and dynamin[7] functions. Recently,

a natural product Ikarugamycin (IKA) has been used to inhibit CME in different systems, but neither its potency nor specificity toward CME have been examined[9]. Typically, the plant cell biology has taken advantage of TyrphostinA23 (TyrA23), a small CME-inhibiting molecule[10]. However, TyrA23 has recently been described as a protonophore in *Arabidopsis thaliana*, that completely inhibit endocytosis through cytoplasmic acidification[10]. As none of the currently available small molecules have been applied widely[11-14], the CME research would benefit from novel and potent small molecule inhibitors that would help in the molecular and functional dissection of the endocytic pathway to improve our understanding of many physiological processes that rely on this pathway.

Previously, the small molecule endosidin9 (ES9) had been identified as an endocytosis inhibitor in different model systems[10]. Although ES9 is primarily a protonophore, cytosol acidification did not seem to be the sole reason for the endocytosis inhibition, because in *Drosophila menalogaster*, ES9 blocked synaptic vesicle recycling, similarly to mutants defective in clathrin or dynamin functions[15,16] and in *Arabidopsis,* ES9 retained the ability to inhibit endocytosis at an increased apoplastic pH[10]. These results suggested that, despite its protonophore activity, ES9 might target proteins involved in CME. Here, we identified CHC as the protein target of ES9. Structural activity relation (SAR) analysis of ES9 resulted in the identification of the improved ES9-17 analog that inhibited endocytosis, but without protonophore activity. *In vivo* target validation strategies, including cellular thermal shift assay (CETSA)[17] and Drug Affinity Responsive Target Stability (DARTS)[18] characterized CHC as a potential target of ES9-17. Hence, we present a useful clathrin-specific CME inhibitor.

Results

ES9 targets CHC. Although the small molecule ES9 **(1)** had been previously characterized as a protonophore and unspecific inhibitor of CME[10], not all ES9-induced phenotypes were explained by its protonophore activity, implying that ES9 might inhibit CME through a direct interaction with its machinery[10]. To explore this possibility, we analyzed ES9 with SAR **(Supplementary Fig. 1a)** to identify a suitable position for derivatization with a linker and a biotin tag and to carry out an affinity-based target identification. A small collection of commercially available and synthetic ES9 analogs was investigated for their ability to inhibit the uptake of the lipophilic styryl endocytic tracer dye *N*-(3-triethylammoniumpropyl)-4-(6-(4-(diethylamino) phenyl)hexatrienyl)pyridinium dibromide (FM4-64)[19] in *Arabidopsis* root epidermal cells at a concentration of 50 μM and 30 min of treatment (**Supplementary Fig. 1a, b**). The partial structure or possible hydrolysis products ES9-3 **(2)** and ES9-7 **(3)** lacked activity in this endocytosis inhibition assay. Methylation of the acidic NH position in ES9-6 **(4)** resulted in FM4-64 uptake and, thus, loss of activity. Replacement of the bulky bromine substituent on the thiophene ring by a hydrogen produced a simplified analog ES9-2 **(5)** that retained activity, hinting at a suitable anchoring place to introduce a linker moiety for a biotin label attachment. Replacement of the thiophene ring itself by its phenyl bioisostere gave the active phenylsulfonamide analog ES9-8 **(6)** that readily allowed the further derivatization of the bromine-occupied position, with the synthesis and identification of the active analog ES9-9 **(7)** with a hydroxyl-terminated linker at this position as a consequence. Next, a biotin tag was introduced to generate the ES9-9 biotin-conjugate ES9-10 **(8)**. In contrast to ES9-9, ES9-10 was not active in the FM4-64 uptake inhibition assay, possibly due to the reduced cell permeability of the large biotinylated compound, but was expected to retain binding affinity to its putative biomolecular targets in *Arabidopsis* cell lysates. A linker-biotin probe without the ES9 moiety, ES9-13 **(9),** was included as a negative control in pull-down experiments (**Supplementary Fig. 1a**).

To identify possible targets of ES9, we prepared protein extracts for affinity purification from PSB-D wild type *Arabidopsis* cell cultures. Proteins bound to ES9-10 and ES9-13 were analyzed by means of mass spectrometry. In total, three biological replicates were examined for the ES9-10 affinity purification and the ES9-13 control, each of which represented by three technical repeats. Proteins found only once in the three biological replicates were not considered, resulting in a list of 169 proteins (**Supplementary Table 1**). Proteins were listed based on the number of times they occurred in the different biological and technical replicates and the number of peptides identified. Proteins that were present in the ES9-10, but not in the ES9-13 pull-down, were considered as potential hits. Fewer than 20 proteins were found to meet the set criteria, among which CHC1, an essential CME component. Nevertheless, CHC2 that occurred also in the list, was found in the ES9-13 pull-down as well.

To validate the possible interaction between ES9 and CHC in *Arabidopsis*, we employed the cellular thermal shift assay (CETSA) that monitors target engagement based on small molecule-induced changes in the thermal stability of protein targets[17]. The aggregation temperature (T_{agg}) of the CHC was assessed through Western blot analysis of *Arabidopsis* cell culture lysates treated with DMSO for 30 min and heated for 2 min at 12 different temperature points (30-65°C). Thermal denaturation of CHC under control (DMSO) conditions indicated a T_{agg} of 45 ±0.23°C (**Fig. 1a**). For further isothermal dose-response fingerprint ($ITDRF_{CETSA}$) experiments of CHC in the presence of ES9, we set the temperature at 46°C to ensure a sufficient shift in the denaturation temperature and determined the half maximum effective concentration (EC_{50}) to be 120.5 ±1.09 μM (**Supplementary Fig. 2a**). In contrast, the control protein ATPβ was largely unaffected, even at high compound concentrations. Although the EC_{50} for the thermal denaturation of CHC in the presence of ES9 was 120 μM, a higher concentration of 250 μM ES9 was used for CETSA to achieve sufficiently sized T_{agg} shifts. The presence of 250 μM ES9 for 30 min and heating for 2 min at

12 different temperature points (30-65°C) generated a lower T_{agg} of 43 ±0.29°C than that of the vehicle control (45 ±0.23°C) that resulted in a T_{agg} shift of 2°C (**Fig. 1a**). Thermal denaturation of the control proteins, tubulin and ATPβ, showed negligible T_{agg} shifts in the presence of either 250 µM ES9 or the vehicle (**Fig. 1b; Supplementary Fig. 2b**). Moreover, in the presence of the inactive analog ES9-6 (250 µM), the T_{agg} for CHC did not differ in the lysates treated with DMSO (44.76±0.47 °C) and ES9-6 (44.49±0.27 °C) **Supplementary Fig. 2c**). These results were corroborated by means of the Drug Affinity Responsive Target Stability (DARTS)[18] to determine the potential of ES9 to protect CHC from protease digestion (**Fig. 1c**). In the presence of ES9 (250 µM), CHC was stabilized at two pronase concentrations when compared to the DMSO-treated control samples. Such stabilization was not observed for the control protein ATPβ (**Fig. 1c**). Taken together, our data indicate that in *Arabidopsis* cells CHC is probably the target of ES9.

ES9 binds the nTD of CHC. In an attempt to predict the binding site of ES9 on CHC, ES9 was docked to the structure of the nTD of the human CHC1 in a complex with either Pitstop1 (pdb2XZG) or Pitstop2 (pdb4G55)[6]. The obtained prediction with pdb4G55 suggested that the binding site for ES9 on CHC1 might be same as that for Pitstop2 (**Supplementary Fig. 3a**). Residues Arg64, Phe91 and Gln89 in the binding site were set as flexible during docking and the first nine predicted positions were all similar, except for minor reorientations of the flexible residues. To confirm this prediction, the highly homologous β-propeller nTDs of both the *Arabidopsis* and the human CHC1 (**Supplementary Fig. 3b)** were produced and the respective protein-ES9 interactions were analyzed *in vitro* by means of differential scanning fluorimetry (DSF) and microscale thermophoresis (MST). Upon ES9 binding to the nTD of the *Arabidopsis* CHC1, DSF detected a shift in the thermostability of CHC1, resulting in a change in its melting temperature (ΔTm) (**Fig. 1d; Supplementary Table 2)**. In contrast, the

thermal denaturation curve for the inactive analog ES9-6 (80 μM) overlapped with that of the (DMSO) control (**Fig. 1d**). The ΔTm measured for the nTD of the human CHC1 had a protein stability in the presence of ES9 similar to that of the nTD of the *Arabidopsis* CHC1 (**Supplementary Fig. 2d; Supplementary Table 2**). Altogether, our results demonstrate that ES9 binds to the nTD of CHC1 both in *Arabidopsis* and in human.

To understand the molecular basis of this interaction, the binding site of ES9 in the nTD of CHC was mapped by determining the structure of the human nTD of CHC1 in a complex with ES9 by protein X-ray crystallography (**Fig. 2a**). Crystals with the clathrin nTD diffracted up to a resolution of 1.6Å and the structure was solved by molecular replacement with the CHC1 nTD as a search model. The CHC1 nTD forms a seven-bladed β-propeller, each with four antiparallel strands. The electron density for ES9 could be identified between the first and second blades (**Fig. 2b**). Modeling of ES9 into this electron density revealed that the ES9-binding site on the CHC nTD overlaps with the binding site for the CME adaptor proteins harboring a clathrin box motif[20]. ES9 is positioned in the cavity formed by four amino acids (Arg64, Ile93, Phe91, Gln89, and Ile66). The conformation of ES9 is stabilized by the electrostatic interactions between the benzonitro moiety of ES9 and Arg64 and the thiophene group of ES9 with the carboxyl oxygen of Ser67 (**Fig. 2c,d**). Thus, the crystal structure analysis corroborated the previous docking predictions that ES9 targets the Pitstop2-binding site[6] in the nTD of CHC.

Identification of the nonprotonophore ES9-17. Although ES9 bound CHC, its protonophore activity[10] limited the use of this small molecule as a specific CME inhibitor. With the aim to uncouple the CHC binding of ES9 from its protonophore CME inhibitory effects, we carried out a SAR analysis to identify ES9 analogs that had lost the protonophore activity, but had retained the ability to inhibit the FM4-64 uptake at 50 μM and applied for

30 min. (**Supplementary Fig. 4a**). As charge distribution over a large area surrounded by hydrophobic aromatic groups is known to allow protonophore activity[21], we attempted to influence the acidity of the sulfonamide of ES9. We assessed both the FM4-64 uptake inhibition and the impact on the mitochondrial membrane potential as visualized with MitoTracker Red CM-H2XRos dye[22] in *Arabidopsis* root epidermal cells **(Supplementary Fig. 4b, c)**. Removal of the acidic NH in ES9-6 already proved detrimental to the FM4-64 uptake inhibitory activity. Transfer of the nitro group from the para to the meta position in ES9-29 **(10)** is expected to make the sulfonamide less acidic, while preserving specific contacts with target biomolecules. However, ES9-29 retained its protonophore activity, indicating that the sulfonamide was still fairly acidic. Other substitutions on the phenyl ring, ES9-15 **(11)** and ES9-16 **(12)** led to loss of the FM-64 uptake blocking activity. Altogether elimination of the nitro group in ES9 should strongly shift the equilibrium toward the protonated form, but it could affect the binding affinities for biomolecular targets. We found that ES9-14 **(13)** (**Supplementary Fig. 4a)** and ES9-17 **(14)** (**Fig. 3a**) both remained active in the FM4-64 uptake inhibition assay and did not prevent the MitoTracker Red CM-H2XRos staining of the mitochondria at 50 μM (**Supplementary Fig. 4b, c)**. Although, ES9-17 inhibited the FM4-64 uptake in *Arabidopsis* root epidermal cells with a IC_{50} of 13 μM (**Fig. 3b**), a concentration of 30 μM was used for further cellular analysis to ensure a substantial reduction in endocytosis (**Fig. 3c**).

To rule out the protonophore activity of ES9-17, we assessed its capacity to affect the cellular ATP in dark-grown *Arabidopsis* PSB-D cell cultures when used at 30 μM together with ES9 (10 μM) and the inactive analog ES9-6 (50 μM) (**Fig. 3d)**. As expected and in contrast to the sharp ATP decrease after treatment with 10 μM ES9 (ref. 10), 30 μM of ES9-17 failed to deplete ATP, as did ES9-6. All small molecules increased the fluorescein diacetate (FDA) fluorescence over time, indicating a lack of cytotoxicity (**Supplementary**

Fig. 5a). Previously, the protonophore activity of ES9 had been shown to be unspecific to the mitochondria, because ES9 acidified the cytoplasm probably through dissipation of the proton gradients over the plasma membrane (PM)[10]. Therefore, we assessed whether ES9-17 affected the cytoplasmic pH. *Arabidopsis* seedlings were preincubated with Lyso Tracker Red DND 99 (ref. 23) to label membranes delineating acidic compartments, followed by a 30-min incubation with DMSO, 10 μM ES9 or 30 μM ES9-17 (**Fig. 3e**). As anticipated, 10 μM of ES9 relocated Lyso Tracker Red DND 99 predominantly to the cytosol when compared to the DMSO control, whereas 30 μM of ES9-17 failed to induce a similar staining pattern. Furthermore, unlike ES9, application of ES9-17 (30 μM for 30 min) did not compromise the motility of the actin cytoskeleton (Fimbrin-GFP)[24], microtubules (MAP4-GFP)[X], the Golgi (ST-Mrfp)[25] and the *trans*-Golgi network (TGN)/early endosome (EE) compartments (VHA-a1-GFP[26] (**Supplemental Fig. 5b-e**).

ES9-17 is a CME inhibitor. To characterize ES9-17 as a CME inhibitor, we evaluated the internalization of several PM-localized cargos subjected to CME in *Arabidopsis* and human cells. We assessed whether the CME-mediated uptake of the brassinosteroid (BR) receptor BRASSINOSTEROID INSENSITIVE 1 (BRI1)[27] would be affected by ES9-17. *Arabidopsis* seedlings expressing GFP-tagged *BRI1*[28] were pretreated for 1 h with 50 μM cycloheximide (CHX) to reduce the amount of newly synthesized proteins, followed by treatments with DMSO or ES9-17 (30 μM) for 30 min and then with 50 μM Brefeldin A (BFA) and FM4-64 for 30 min. In the presence of ES9-17, BRI1-GFP failed to label the BFA body (**Fig. 4a**), hinting at an inhibition of the BRI1-GFP uptake from the PM. The lack of BRI-GFP-labeled BFA bodies was not due to a limitation of the BFA body formation by ES9-17, because BFA bodies marked by the TGN/EE marker VHAa1-GFP[26] could be formed, whereas the FM4-64 uptake was inhibited (**Supplementary Fig. 6a**). Furthermore, fluorescently labeled Alexa

fluor 674 castasterone (AFCS), which binds to BRI1 and consequently enters the cell through CME[27], failed to stain the vacuole in root epidermal cells when applied to *Arabidopsis* seedlings expressing BRI1-GFP[28] after pretreatment with 30 μM ES9-17 for 30 min (**Supplementary Fig. 6b**). To corroborate the CME inhibition by ES9-17, we examined another PM-localized cargo, which is subject to CME, the leucine-rich repeat receptor kinase PEP RECEPTOR1 (PEPR1)[29]. Treatment of *Arabidopsis* root cells expressing PEPR1-GFP with 1 μM of the AtPep1 peptide for 10 sec after pretreatment with DMSO for 30 min induced PEPR1-GFP internalization (**Fig. 4b**). However, when roots were pretreated with 30 μM ES9-17 for 30 min and elicited with 1 μM AtPep1, PEPR1-GFP was still predominantly localized to the PM even 90 min after the elicitation, implying an inhibitory effect of ES9-17 on the CME-mediated PEPR1 uptake (**Fig. 4b).**

Furthermore, we analyzed the effect of ES9-17 on the uptake of transferrin in HeLa cells, known to be a clathrin-mediated process[30]. Treatment of HeLa cells with 30 μM ES9-17 for 30 min inhibited the uptake of transferrin to an extent similar to that of 20 μM Pitstop2 (**Fig. 4c; Supplementary Fig. 6c**). In parallel with the inhibitory treatments, a cell proliferation assay was conducted to ascertain that the resulting inhibition of the transferrin uptake was not due to the cytotoxicity of the compounds (**Supplementary Fig. 6d**).

To characterize the effect of ES9-17 on CME, we evaluated the dynamic behavior of known components of CME in root epidermal cells of *Arabidopsis*. We chose for clathrin, CLC1-GFP[10] and CHC1-GFP[10], and for the TPLATE muniscin-like (TML) subunit of the TPLATE complex (TPC)[31] as representative for the CME adaptor proteins in plants. In the presence of DMSO, the majority of the PM-localized foci had an average residence life time of xx.xx sec, 44.62 sec and 36.72 sec for CLC1-GFP, CHC1-GFP and TML-GFP, respectively (**Fig. 4d; Supplementary Fig. 6e, f**). When seedlings were treated with 30 μM ES9-17, the residence life time of CHC1, CHC1 and TML in the PM increased substantially

with an average of xx.xx sec, 83.55 sec and 68.66 sec, respectively (**Fig. 4d; Supplementary Fig. 6e, f**). Taken together, ES9-17 inhibited the uptake of several CME cargos in *Arabidopsis*, it affected the dynamic behavior of several CME components at the PM, and inhibited the transferrin uptake in HeLa cells to an extent comparable to that of the known CME inhibitor Pitstop2.

ES9-17 possibly targets CHC. As ES9-17 inhibited several clathrin-dependent processes and the parent molecule ES9 bound CHC1, we hypothesized that CHC might also be the target of ES9-17. To test this hypothesis, we made use of the target validation approaches CETSA and DARTS. $ITDRF_{CETSA}$ analysis at 46°C indicated an EC_{50} of 123±1.13 µM for ES9-17 (**Supplementary Fig. 7a**), which is very close to the EC_{50} observed for ES9. Similarly, as observed for ES9, a shift in T_{agg} for CHC was detected in the presence of ES9-17. *Arabidopsis* cell culture lysates treated with DMSO (Ø) for 30 min and heated for 2 min at 12 different temperature points (30-65°C) resulted in a T_{agg} for CHC of 44.96±0.2°C, whereas in the presence of 250 µM ES9-17 the T_{agg} was 42.71±0.2°C, thus generating a T_{agg} shift of 2.2°C (**Fig. 5a**). In contrast, ES9-17 failed to induce a shift in T_{agg} for the control proteins, tubulin and ATPβ (**Fig. 5b; Supplementary Fig. 7b**). These results were supported by the DARTS assay, in which cell lysates treated with ES9-17 (250 µM) exhibited a significant stabilization of the endogenous full-length CHC at reduced dilutions of pronase, but not by the control protein ATPβ (**Fig. 5c**). At pronase concentrations of 1:4000 and 1:2000, a 2-fold and 1.5-fold stabilization was observed for CHC in ES9-17-treated cell lysates, respectively. To confirm the results obtained with the CETSA and DARTS assays, we tried to assess genetically whether ES9-17 interacted with CHC. In contrast to ES9, of which the protonophore activity prevents meaningful genetic studies, ES9-17 lacks the protonophore characteristics and, hence, can be used to evaluate the increased sensitivity or resistance of mutant alleles.

However, double knockout mutant lines, for which resistance to ES9-17 might be expected, cannot be used, because CHC has an essential function. Therefore, several single mutant alleles for *CHC1* and *CHC2* (ref. 23) were examined for their higher sensitivity to ES9-17 than that of the wild type. Primary root growth for 5-day-old *Arabidopsis* (accession Columbia-0) seedlings was inhibited with an EC_{50} of 9 μM (**Supplementary Fig. 7c**). To assure a sufficient root growth inhibition, we set the concentration of ES9-17 at 12 μM. Seedlings of *chc1-3*, *chc2-1* and *chc2-2* mutant lines displayed a significantly increased sensitivity to ES9-17 compared to the Col-0 seedlings (**Fig. 5d; Supplementary Fig. 7d**). Root growth did not significantly vary for the different mutant alleles when compared to Col-0, when grown under control conditions. Taken together, the results obtained with CETSA, DARTS and CHC mutant alleles point toward CHC as one of the possible protein targets of ES9-17 in *Arabidopsis*.

Discussion

In plants, CME is one of the most studied pathway for internalization of membrane-associated and soluble cargos from the PM and the extracellular environment[1]. As loss-of-function CME mutants are often lethal or have no phenotypes because of gene redundancy[32], methods to perturb CME largely rely on the use of inducible expression of mutant forms of critical proteins involved in endocytosis, such as clathrin and auxillin[33,34], and siRNA-mediated depletion of adaptor proteins, such as TPC[31]. The drawbacks of this approach are the low gene induction efficiency, the construct silencing and the considerable time needed to deplete a cell from these proteins (2-5 days), while the cell may adapt and even alter the gene expression, without certitude that only CME is impacted. Loss of a protein, such as clathrin, might impair post-Golgi trafficking[35] with possible defects in secretion and vacuolar targeting

as a consequence. Therefore, application of small molecule inhibitors of CME combined with live-cell imaging can greatly facilitate studies of the CME machinery and dynamics. An attractive feature of chemical inhibitors is that they may be applied acutely to reveal the direct block of a particular process. Reversibility of the inhibition can also support the specific impact on the particular mode of endocytosis that is examined[36].

Over the years, different small molecule effectors of endocytosis and endosomal function in *Arabidopsis* have been described, including several from the endosidin (ES) family[37]. A subset of ES molecules, ES2 and ES16, have been shown to affect post-Golgi trafficking, including exocytosis and endosome function[38,39]. The identification and characterization of the CME inhibitor ES9 (ref. 10) revealed that the mode of action of this compound is mediated via its mitochondrial uncoupling and protonophore activities, therefore causing ATP depletion and cytoplasmic acidification. This mode of action appeared to be shared with the until then most commonly used plant CME inhibitor, TyrA23. Therefore, in contrast to mammalian systems, in which the small CME inhibitors Pistop2 and Dynasore are well established[6,7], plant systems lack small molecules that specifically target the CME machinery and inhibitors, such as Pistop2 and Dynasore, seem to be less active in plants[10]. Although ES9 acts as a protonophore, evidence suggested that ES9 may have CME inhibiting effects beyond those resulting from cytoplasmic acidification[10], prompting an affinity-based target identification strategy that identified CHC1 as a possible ES9-binding protein. Subsequent validation with both *in vivo* techniques, such as CETSA[17] and DARTS[18], and *in vitro* methods, including MST and DSF, revealed that ES9 binds the *Arabidopsis* and human nTD of CHC. This interaction was confirmed by the crystal structure of the human nTD of CHC with ES9, revealing that ES9 binds the same clathrin box as Pitstop2 (ref. 6), positioned between blade 1 and 2 of the nTD β-propeller. Although only CHC1 seems to be a main hit after affinity purification, both CHC1 and CHC2 interacted with ES9 in *in vitro* studies. The

reason for this apparent discrepancy might be either the low CHC2 abundance or its reduced affinity in binding to the biotin-tagged ES9.

Despite the binding of ES9 to CHC, its use as a specific inhibitor of the CHC function is hampered by its protonophore characteristics. Nevertheless, the discovery that ES9 binds clathrin opened up the possibility to develop nonprotonophoric CME inhibitors through SAR analysis with ES9 as a scaffold, leading to the identification of ES9-17. ES9-17 lacked the nitro group of ES9 and, hence, lost its ability to act as a protonophore, as confirmed by the lack of ATP depletion and by the membrane potential-dependent staining of mitochondria in *Arabidopsis* in the presence of ES9-17. This compound retained, however, the ability to inhibit the uptake of FM4-64 and of several CME cargos in *Arabidopsis*, validating ES9-17 as an inhibitor of receptor-mediated endocytosis. Moreover, the CME inhibition was not restricted to *Arabidopsis*, because ES9-17 impaired the transferrin uptake in HeLa cells. Similarly to the previously reported CME inhibitors from the Pitstop family[6], ES9-17 increased the dwell time of the endocytic foci in the PM, in contrast to the general freeze in foci dynamics observed with ES9 (ref. 10). In addition, ES9-17 lacked the ability to acidify the cytoplasm and, thus, to hamper endomembrane compartment motility and cytoplasmic streaming, as visualized by the TGN/EE, Golgi and cytoskeleton dynamics and the overall Golgi, TGN/EE and BFA body morphology.

However, the validation strategy for ES9-17, similar to that used for ES9, indicated binding to CHC in the CETSA and DARTS assays, but failed to show interaction with CHC in *in vitro* and crystallographic studies with both *Arabidopsis* and human nTD CHC (data not shown). A possible explanation lies in the presence of the nitro group of ES9 that establishes an interaction with Arg64 of the nTD, but is absent in ES9-17 (**Supplementary Fig. 3a)**. Therefore, ES9-17 is probably unable to strongly interact with the nTD. Alternatively, we cannot exclude the possibility that ES9-17 targets other CHC domains or that it, requires

accessory adaptor proteins for binding to CHC, although ES9-17 did not bind to tested TPC or adaptor protein complex-2 subunits alone (**Supplementary Fig. 7e-g)**. In addition, in contrast to ES9, the reduced solubility and overall availability of ES9-17 when used in *in vitro* assays might have affected the positive outcome of these experiments.

Remarkably, the results obtained with CETSA for ES9-17 are very similar to those for ES9. Both the temperature shift in the CHC denaturation and the EC_{50} concentration for ES9-17 and ES9 were essentially the same, strongly suggesting that ES9-17 might indeed bind CHC. This trend extends to the DARTS analysis, in which, compared to ES9, ES9-17 induced a similar protection from the protease digestion of CHC. In addition, knockout mutants of CHC showed a significant increase in root growth sensitivity when grown on ES9-17, adding genetic evidence to the argument that ES9-17 binds CHC.

In summary, we established that the unspecific CME inhibitor ES9 also targets CHC. However, the use of this small molecule is complicated, because ES9 also acts as a protonophore. The identification of the nonprotonophoric analog ES9-17 has provided an additional endocytosis inhibitor that specifically targets the CME machinery. In addition, the ES9-17 activity is not restricted to *Arabidopsis*, because it was also active in HeLa cells. This observation opens the opportunity to develop and characterize ES9-17 in mammalian systems. In *Arabidopsis*, future work will emphasize on the full identification of ES9-17, including the binding site on CHC. In turn, additional ES9 analogs could be designed and developed that might possess an increased affinity toward CHC or allow the distinction between CHC1 and CHC2. Ultimately, ES9 and its analogs will provide a detailed dissection of the CHC function in *Arabidopsis,* both in a CME context and beyond.

Methods

Methods, including statements of data availability and any associated accession codes and references, are available in the online version of the paper.

References

1. Reynolds, G.D., Wang, C., Pan, J. & Bednarek, S.Y. Inroads into internalization: five years of endocytic exploration. *Plant Physiol*. **176**, 208-218 (2018).
2. Kaksonen, M. & Roux, A. Mechanisms of clathrin-mediated endocytosis. *Nat. Rev. Mol. Cell Biol*. **19**, 313-326 (2018).
3. Mettlen, M., Chen, P.-H., Srinivasan, S., Danuser, G. & Schmid, S.L. Regulation of clathrin-mediated endocytosis. *Annu. Rev. Biochem*. **87**, in press (doi: 10.1146/annurev-biochem-062917-012644) (2018).
4. Valencia, J.P., Goodman, K. & Otegui, M.S. Endocytosis and endosomal trafficking in plants. *Annu. Rev. Plant Biol*. **67**, 309-335 (2016).
5. Mishev, K., Dejonghe, W. & Russinova, E. Small molecules for dissecting endomembrane trafficking: a cross-systems view. *Chem. Biol*. **20**, 475–486 (2013).
6. von Kleist, L. *et al*. Role of the clathrin terminal domain in regulating coated pit dynamics revealed by small molecule inhibition. *Cell* **146**, 471-484 (2011).
7. Macia, E. *et al*. Dynasore, a cell-permeable inhibitor of dynamin. *Dev. Cell* **10**, 839-850 (2006).
8. McCluskey, A. *et al*. Building a better dynasore: the Dyngo compounds potently inhibit dynamin and endocytosis. *Traffic* **14**, 1272-1289 (2013).
9. Elkin, S.R. *et al*. Ikarugamycin: a natural product inhibitor of clathrin-mediated endocytosis. *Traffic* **17**, 1139-1149 (2016).
10. Dejonghe, W. *et al*. Mitochondrial uncouplers inhibit clathrin-mediated endocytosis largely through cytoplasmic acidification. *Nat. Commun.* **7**, 11710 (2016).

11. Dutta, D., Williamson, C.D., Cole, N.B. & Donaldson, J.G. Pitstop 2 is a potent inhibitor of clathrin-independent endocytosis. *PLoS ONE* **7**, e45799 (2012).

12. Willox, A.K., Sahraoui, Y.M.E. & Royle, S.J. Non-specificity of Pitstop 2 in clathrin-mediated endocytosis. *Biol. Open* **3**, 326-331 (2014).

13. Park, R.J. *et al*. Dynamin triple knockout cells reveal off target effects of commonly used dynamin inhibitors. *J. Cell Sci*. **126**, 5305-5312 (2013).

14. Preta, G., Cronin, J.G. & Sheldon, I.M. Dynasore - not just a dynamin inhibitor. *Cell Commun. Signal*. **13**, 24 (2015).

15. Kasprowicz, J. *et al*. Inactivation of clathrin heavy chain inhibits synaptic recycling but allows bulk membrane uptake. *J. Cell Biol*. **182**, 1007-1016 (2008).

16. Heerssen, H., Fetter, R.D. & Davis, G.W. Clathrin dependence of synaptic-vesicle formation at the *Drosophila* neuromuscular junction. *Curr. Biol*. **18**, 401-409 (2008).

17. Jafari, R. *et al*. The cellular thermal shift assay for evaluating drug target interactions in cells. *Nat. Protoc*. **9**, 2100 (2014).

18. Lomenick, B. *et al*. Target identification using drug affinity responsive target stability (DARTS). *Proc. Natl. Acad. Sci. USA* **106**, 21984-21989 (2009).

19. Jelínková, A. *et al*. Probing plant membranes with FM dyes: tracking, dragging or blocking? *Plant J*. **61**, 883-892 (2010).

20. Popova, N.V., Deyev, I.E. & Petrenko, A.G. Clathrin-mediated endocytosis and adaptor proteins. *Acta Naturae* **5**, 62-73 (2013).

21. Onizuka, S., Ikewaki, N. & Shiraishi, S. A mechanism by which propofol induces cytotoxicity. *J. Drug Metab. Toxicol*. **8**, 230 (2017).

22. Poot, M. *et al*. Analysis of mitochondrial morphology and function with novel fixable fluorescent stains. *J. Histochem. Cytochem*. **44**, 1363-1372 (1996).

23. Dolman, N.J., Kilgore, J.A. & Davidson, M.W. A review of reagents for fluorescence microscopy of cellular compartments and structures, Part I: BacMam labeling and reagents for vesicular structures. *Curr. Protoc. Cytom*. **65**, 12.30.1-12.30.27 (2013).

24. Wang, Y.-S., Yoo, C.-M. & Blancaflor, E.B. Improved imaging of actin filaments in transgenic *Arabidopsis* plants expressing a green fluorescent protein fusion to the C- and N-termini of the fimbrin actin-binding domain 2. *New Phytol*. **177**, 525-536 (2008).

25. Teh, O.-k. & Moore, I. An ARF-GEF acting at the Golgi and in selective endocytosis in polarized plant cells. *Nature* **448**, 493-496 (2007).

26. Dettmer, J., Hong-Hermesdorf, A., Stierhof, Y.-D. & Schumacher, K. Vacuolar H^+-ATPase activity is required for endocytic and secretory trafficking in *Arabidopsis*. *Plant Cell* **18**, 715-730 (2006).

27. Irani, N.G. *et al*. Fluorescent castasterone reveals BRI1 signaling from the plasma membrane. *Nat. Chem. Biol*. **8**, 583–589 (2012).

28. Friedrichsen, D.M., Joazeiro, C.A.P., Li, J., Hunter, T. & Chory, J. Brassinosteroid-insensitive-1 is a ubiquitously expressed leucine-rich repeat receptor serine/threonine kinase. *Plant Physiol*. **123**, 1247-1255 (2000).

29. Ortiz-Morea, F.A. *et al*. Danger-associated peptide signaling in *Arabidopsis* requires clathrin. *Proc. Natl. Acad. Sci. USA* **113**, 11028-11033 (2016).

30. Tacheva-Grigorova, S.K., Santos, A.J.M., Boucrot, E. & Kirchhausen, T. Clathrin-mediated endocytosis persists during unperturbed mitosis. *Cell Rep*. **4**, 659-668 (2013).

31. Gadeyne, A. *et al*. The TPLATE adaptor complex drives clathrin-mediated endocytosis in plants. *Cell* **156**, 691-704 (2014).

32. Kitakura, S. *et al*. Clathrin mediates endocytosis and polar distribution of PIN auxin transporters in *Arabidopsis*. *Plant Cell* **23**, 1920-1931 (2011).

33. Dhonukshe, P. *et al*. Clathrin-mediated constitutive endocytosis of PIN auxin efflux carriers in *Arabidopsis*. *Curr. Biol*. **17**, 520-527 (2007).

34. Adamowski, M. *et al.* A functional study of AUXILIN-LIKE1 and 2, two putative clathrin uncoating factors in Arabidopsis. *Plant Cell* **30**, 700-716 (2018).

35. Robinson, D.G. & Pimpl, P. Clathrin and post-Golgi trafficking: a very complicated issue. *Trends in Plant Science*, **19**, 134-139 (2014).

36 Hicks, G.R. & Raikhel, N.V. Small molecules present large opportunities in plant biology. *Annu. Rev. Plant Biol*. **63**, 261-282 (2012).

37. Drakakaki, G. *et al*. Clusters of bioactive compounds target dynamic endomembrane networks in vivo. *Proc. Natl. Acad. Sci. USA* **108**, 17850-17855 (2011).

38. Zhang, C. *et al*. Endosidin2 targets conserved exocyst complex subunit EXO70 to inhibit exocytosis. *Proc. Natl. Acad. Sci. USA* **113**, E41-E50 (2016).

39. Li, R. *et al*. Different endomembrane trafficking pathways establish apical and basal polarities. *Plant Cell* **29**, 90-108 (2017).

Acknowledgements

We thank Steffen Vanneste for useful discussion and materials, Rahul Kumar for providing the pDONR211AP2S construct, Daniel Martinez Molina for help with the CETSA protocol and Martine De Cock for help in preparing the article. This work was supported by Research Foundation-Flanders (project no. G022516N to E.R.), by the Agency for Innovation by Science and Technology (IWT) for a postdoctoral (K.M.) and predoctoral (W.D.) fellowship; the China Science Council for a predoctoral fellowship (Q.L.); a joint research project (VS.025.13N) within the framework of cooperation between the Research Foundation-Flanders and the Bulgarian Academy of Sciences (K.M. and E.R.) and the Belgian Science Policy Office (BELSPO) for a postdoctoral fellowship to non-EU researchers (I.S.).

Author contributions

W.D. and E.R. initiated the work; W.D., I.S., and E.R. designed the experiments; W.D., I.S., B.D., A.M., and J.W. did SAR; W.D., K.M., A.S. and K.G. did affinity purification and MS analysis; H.B. and V.H. performed the X-ray crystallography; I.S., S.D.M. and S.S. did *in vitro* binding assay; W.N. did molecular docking; W.D. and I.S. did CETSA; I.S. and Q.L. did DARTS; I.S., D.V.S., E.M., and D.V.D. did imaging and data analysis; I.S. did cloning and generated transgenic *Arabidopsis* cell cultures; W.D., I.S., A.D., and D.A. did ATP measurements; M.V. and J.F. contributed the HeLa cells assays; W.D., I.S. and E.R. wrote the manuscript. All authors commented on the results and the manuscript.

Competing financial interests

The authors declare no competing financial interests: details accompany the online version of the paper.

Additional information

Any supplementary information, chemical compound information and source data are available in the online version of the paper. Reprints and permissions information is available online at http://www.nature.com/reprints/index.html. Publisher's note: Springer Nature remains neutral with regard to jurisdictional claims in published maps and institutional affiliations. Correspondence and requests for materials should be addressed to E. R.

Methods

Plant material and growth conditions. *Arabidopsis thaliana* (L.) Heyhn. (accession Columbia-0 [Col-0]) seedlings and other lines were stratified for 2 days at 4°C and grown vertically on agar plates containing half-strength Murashige and Skoog (½MS) medium supplemented with 1% (w/v) sucrose for 5 days at 22°C in a 16-h/8-h light/dark cycle, prior to use. The *Arabidopsis* mutants and transgenic lines used were: *chc2-1* (ref. 32), *chc2-2* (ref. 32), TML-GFP[31], CHC2-GFP[10], CHC1-GFP[10], VHA-a1-GFP[26], ST-mRFP[25], PEPR1-GFP[29], BRI1-GFP[28] and Fimbrin-GFP[24]. The *chc1-3* allele…

Generation of hemagglutin (HA)-tagged AP2S and AP2M constructs and *Arabidopsis* PSB-D cell culture transformation. Entry clones pDONRRP4-1R_RPS5A[10], pDONRRP2R-P3_HAstop and pDONR211_AP2S (AT1G47830) or pDONR211_AP2M^{X} (AT5G46630) were used together with pH7m34GW in multisite Gateway reactions (Life Technologies) to generate the pRPS5A-AP2S-HA and pRPS5A-AP2M-HA constructs. The AP2M-HA and AP2S-HA expression vectors were used to transform *Agrobacterium tumefaciens* C58. The PSB-D wild type cell cultures were subsequently transformed as described[40].

Chemical treatments, chemical labeling and imaging in *Arabidopsis.* ES9 and analogs were acquired through Chembridge (http://www.chembridge.com/) or synthesized. Compounds were dissolved in DMSO (Sigma-Aldrich) and 50 mM stocks were stored at -20°C in glass vials. ES9-17 was freshly prepared from lyophilized powder (stored at -20°C) prior to use. Brefeldin A and cycloheximide (Sigma-Aldrich) were dissolved in DMSO. Endocytosis was visualized with 2 μM FM4-64 (Life technologies). For staining of mitochondria, seedlings were first treated for 30 min in ¼ MS (a 1:1 dilution of ½MS with water) with the respective small molecules and subsequently transferred to liquid ¼MS with 250 nM MitoTracker Red CM-H2XRos (Molecular Probes®, Life Technologies) for an additional 30 min. Similarly, acidic compartments were labeled with Lyso Tracker Red DND

99 (Molecular Probes®, Life Technologies) by treating seedlings with 250 nM Lyso Tracker Red DND 99 in liquid ¼MS for 30 min, followed by a 30-min treatment with small molecules. To observe the internalization of AFCS, seedlings expressing BRI1-GFP were treated with ES9-17 for 30 min followed by 20 µM of AFCS for 20 min. Seedlings were then quickly washed for 20 min. To follow the PEPR1-GFP internalization, seedlings expressing PEPR1-GFP were treated with ES9-17 for 30 min followed by elicitation with AtPep1 (100 nM) for 10 sec. Seedlings were then treated with 2 µM FM4-64 for 30 min and then imaged for different time points. Seedlings were imaged with an Olympus FV10 ASW confocal laser scanning microscope with a 60× water immersion lens (NA 1.2) and 3× digital zoom. Life-time endocytic foci were measured with a Perkin Elmer Ultra View Vox Spinning disc confocal imaging system running on the Volocity software package mounted on a Nikon Eclipse Ti inverted microscope and a Plan Apo Lambda 100× oil (NA 1.45) corrected lens and third-generation perfect focus system (PFSIII) for Z-drift compensation. Time series were acquired at two time points per second intervals, for 5 min. Excitation was done with a solid state 488 nm DPSS laser (50 mW) and images were acquired with a Hamamatsu ImagEM C9100-13 512×512 BI (16 µm × 16 µm pixel size) EmCCD camera. Images were processed by means of the ImageJ (Fiji) software packages.

For the quantification of the PM/cytosol signal intensity ratio, images were converted in ImageJ to 8-bit and regions of interest (ROIs) were selected based on the PM or cytosol localization. Histograms listing all intensity values per ROI were generated and the averages of the 100 most intense pixels were used for calculations.

ATP measurements. Three-day-old wild type PSB-D *Arabidopsis* cell cultures were diluted 100 times and distributed as 95 µl suspension in 96-well plates. Subsequently, 5 µl of a 1/50 dilution of the small molecule stock solution (1000×) in the MS medium with Minimal Organics (MSMO) medium was added to the cells (final dilution of 1000×) by means of a

Tecan Freedom EVO® robot. ATP levels were detected by addition of 80 µl of ATPlite 1step Luminescence Assay System (Perkin Elmer) after incubation of the cells in the presence of the small molecule for the indicated time. Fluorescence was detected with a Perkin Elmer EnVision 2104 multilabel reader with the Wallac Envision manager software package. The fluorescein diacetate (FDA) stock solution (2% [w/v] FDA in acetone; Sigma-Aldrich) was diluted 100× in the target medium and 5 µl was added to 95 µl cell culture. Fluorescence was detected with an excitation at 485 nm (band width 14 nm) and emission at 535 nm (band width 25 nm).

Affinity purification with biotinylated small molecules. PSB-D wild type cell cultures were harvested by separating cells from the medium, flash frozen in liquid nitrogen and ground with a Retsch® MM400. Cell material was weighed and extraction buffer (50 mM Tris-HCl, pH 8, 150 mM NaCl, 0.1% NP-40 [Sigma-Aldrich] with 1 tablet/10 mL cOmplete ULTRA protease inhibitor cocktail, EDTA free [Roche] per 10 ml) was added in 2:1 ratio (200 µl extraction buffer for 100 mg material). Cell material was allowed to thaw on ice for 15 min. Protein concentration was determined with the Bradford method (Quick start Bradford 1× Dye reagent [Bio-Rad]). Lysate was prepared by removing endogenous biotin. To this end, 50 µl of washed (3× with 500 µl extraction buffer, spun down at 1500 rpm, 4°C) Steptavidin Sepharose High Performance beads (GE Healthcare; hereafter referred to as beads) were applied to a 1-ml lysate and incubated at 4°C for 1 h on a rotary wheel. Meanwhile, a second batch of beads was prepared as described above, but biotinylated small molecules (2 µl of 50-mM stock per 50 µl beads) were added with the last wash. The mixture was left at room temperature for 15 min and transferred to 4°C until further use. The bead-incubated lysate was spun down (~~1500 rpm~~ at 4°C) for the removal of biotin, the supernatant collected, and added to beads incubated with the biotinylated small molecules, of which the supernatant was removed after centrifugation (~~1500 rpm~~, 4°C) prior to use. The subsequent mixture was

incubated for a minimum of 2 h, or overnight at 4°C on a rotary wheel, whereafter the mixture was spun down (~~1500 rpm~~, 4°C), the supernatant removed, and washed 3 times (50 mM Tris-HCl, pH 8, 150 mM NaCl). Appropriate amounts of the LDS sample buffer (4× LDS sample buffer supplemented with 10× sample reducing agent; Novex, Life Technologies) were added and samples were incubated for 10 min at 70°C and at ~~350 rpm~~, followed by a 2-min centrifugation at maximum speed. The resulting supernatant was collected and run on 4-12% Bis-Tris protein gels with MES buffer (NuPage Novex gels and buffer from Life technologies). Gels were stained with SYPRO Ruby protein gel stain (Molecular probes, Invitrogen) and stained gel regions were excised and cut in approximately 9 pieces before submission to liquid chromatography-tandem mass spectrometry (LC-MS/MS) analysis.

LC−MS/MS Analysis. Gel pieces containing the proteins of interest were cut from the gel and transferred to Biopure® Eppendorf tubes (Eppendorf AG, Hamburg, Germany). After two consecutive 15-min wash steps with water/acetonitrile (1/1, v/v) (both HPLC analytical; Mallinckrodt Baker B.V., Deventer, The Netherlands), the gel pieces were completely dried in a centrifugal vacuum concentrator, subsequently rehydrated in 10 µl of a 0.02 µg/µl of a sequencing-grade modified trypsin stock solution (Promega Corporation) and, completely submerged under 50 mM of a freshly prepared ammonium bicarbonate solution. The overnight digestion at 37°C was stopped by acidification with TFA. After centrifugation (value?), the peptide mixture was removed from the gel pieces, transferred to a new Eppendorf tube, completely dried in a centrifugal vacuum concentrator and redissolved in 20 µl of 0.1% (w/v?) TFA in water/acetonitrile (98/2, v/v) (loading solvent). The obtained 10-µl peptide mixtures were introduced into an LC−MS/MS system through an Ultimate 3000 RSLC nano LC (Thermo Fisher Scientific) in-line connected to a Q Exactive mass spectrometer (Thermo Fisher Scientific). The sample mixture was first loaded on an in-house made trapping column (100 µm internal diameter [I.D.] × 20 mm, 5 µm beads C18 Reprosil-

HD; Dr. Maisch, Ammerbuch-Entringen, Germany). After flushing from the trapping column, the sample was loaded on an in-house made analytical column (75 µm I.D. × 150 mm, 5 µm beads C18 Reprosil-HD; Dr. Maisch) packed in the needle (PicoFrit SELF/P PicoTip emitter, PF360-75-15-N-5; New Objective, Woburn, MA, USA). Peptides were loaded with loading solvent (0.1% (v/v?) TFA in water/acetonitrile, 2/98 (v/v)) and separated with a linear gradient from 98% solvent A' (0.1% (v/v?) formic acid in water) to 40% solvent B′ (0.1% (v/v?) formic acid in water/acetonitrile, 20/80 (v/v)) in 30 min at a flow rate of 300 nL/min, followed by a 5-min wash, reaching 99% solvent B'. Two packing and two analytical columns were configured in tandem LC mode. Switching between two flow paths, an analysis and a regeneration flow path, allows column washing and reequilibration off-line; thus, while one column is reequilibrated, the system injects a sample on the other column. The mass spectrometer was operated in data-dependent, positive ionization mode, automatically switching between MS and MS/MS acquisition for the 10 most abundant peaks in a given MS spectrum. The source voltage was 3.4 kV and the capillary temperature was 275°C. One MS1 scan (*m/z* 400−2000, AGC target 3 × 106 ions, maximum ion injection time 80 ms) acquired at a resolution of 70,000 (at 200 *m/z*) was followed by up to 10 MS/MS scans (resolution 17,500 at 200 *m/z*) of the most intense ions fulfilling predefined selection criteria (AGC target 5 × 104 ions, maximum ion injection time 60 ms, isolation window 2 Da, fixed first mass 140 *m/z*, spectrum data type: centroid, underfill ratio 2%, intensity threshold 1.7×E4, exclusion of unassigned, 1, 5-8, >8 charged precursors, peptide match preferred, exclude isotopes on, dynamic exclusion time 20 sec). The HCD collision energy was set at 25% Normalized Collision Energy and the polydimethylcyclosiloxane background ion at 445.120025 Da was used for internal calibration (lock mass).

From the MS/MS data in each LC run, Mascot Generic Files (mgf) were created with the Mascot Distiller software (version 2.4.3.3; Matrix Science). These peak lists were then

searched with the Mascot search engine and the Mascot Daemon interface (version 2.4, Matrix Science). Spectra were searched against the TAIR10 database. Variable modifications were set to pyro-glutamate formation of amino-terminal glutamine, acetylation of the protein N terminus, methionine oxidation and propionaide cysteine formation. Mass tolerance on precursor ions was set to ± 10 ppm (with the Mascot C13 option set at 1) and on fragment ions to 20 mmu. The instrument setting was on ESI-QUAD. The enzyme was set to trypsin/P, allowing one missed cleavage, whereas cleavage was allowed also when lysine or arginine was followed by proline. Only peptides that were ranked first and scored above the threshold score, set at 99% confidence, were withheld. All data were managed by ms_lims and analyzed with R (http://www.R-project.org) embedded in KNIME. The data were filtered by removing all peptides smaller than eight amino acids and only the proteins containing at least two peptides in one of the experiments were taken into account for data analysis.

CETSA. The protocol is largely based on that published previously[17] with minor adjustments. Wild type or transgenic *Arabidopsis* PSB-D cell cultures were harvested, flash frozen in liquid nitrogen and ground with a Retsch® MM400. Cell material was weighed and the extraction buffer (50 mM Tris-HCl, pH 7.6, 150 mM NaCl, 0.1% NP-40 with 1 tablet/10 mL cOmplete ULTRA protease inhibitor cocktail, EDTA free (Roche)) was added in a 2:1 ratio. Cell material was allowed to thaw on ice for 15 min with occasional mixing. Samples were centrifuged for 30 min at maximum speed (value?) at 4°C. Lysates were pooled per cell type and the protein concentration was determined with the Bradford method (Quick start Bradford 1× Dye reagent (Bio-Rad)). Pooled lysates were treated with small molecules or mock (DMSO) and incubated for 30 min at room temperature on a rotary wheel. The treated lysates were aliquoted in 60-µl fractions in PCR tubes, treated for 2 min at 12 temperature points (30, 35, 40, 42, 44, 46, 48, 50, 52, 55, 60, and 65°C) in a Bio-Rad thermal cycler, allowed to cool down and centrifuged at maximum speed (value?) for 30 min at 4°C. The supernatant (50 µl)

was taken and processed for standard Western blot analysis to detect the proteins. All antibodies were diluted in TBS-T with 5% (w/v?) skimmed milk. Anti-CHC (1/3000, AS10 690 Agrisera) anti-AtpB (1/4000, AS05085 Agrisera) were detected with horseradish peroxidase (HRP)-linked anti-rabbit IgG (GE Healthcare, 1:10000), anti-tubulin (1/15000) with HRP-linkked anti-mouse IgG (GE Healthcare, 1:10000) and HA with anti-HA-HRP (1/4000, Abcam). Blots were developed with Western Lightning® Plus–ECL, Enhanced Chemiluminescence Substrate (Perkin-Helmer) and imaged with a Bio-Rad ChemiDoc XRS+ molecular imager. Band intensity was measured with the Bio-Rad Image Lab software package.

DARTS. The DARTS protocol was adopted as previously described[18] with the exception of the different used pronase dilutions. Lysates were prepared as described for CETSA. Lysates treated with ES9-17 (250 µM) or mock (DMSO; Sigma-Aldrich) were incubated for 30 min at room temperature. After incubation, lysates were split into equal aliquots for pronase (Roche, 10 165 921 001) digestion. Pronases were diluted from a 10 mg/ml stock solution in dH_2O. The 1/100 starting dilution of pronase that was used for all the subsequent dilutions as indicated was obtained by dissolving 12.5 µl pronase stock solution in 87.5 µl 1× TNC buffer (500 mM Tris-HCl, pH 8, 500 mM NaCl, 100 mM $CaCl_2$, 10× stock). All dilutions were prepared with 1× TNC buffer. Digestion (30 min) was started with 1-min intervals and stopped by addition of the sample buffer at a 1× final concentration (4× LDS sample buffer with 10× sample reducing agent; Novex, Life Technologies) in the same sequence as the digestion had been started. Western blotting, protein detection and quantification were as described for CETSA.

Molecular docking Water and all ligands of the human clathrin nTD crystal structure pdb-entry 4G55 in complex with Pitstop2 (ref. 6) were manually deleted from the pdb-text file. The emptied structure was subjected to a local minimization with the GROMOS96 (43B1

parameter set)[41] implementation within the Swiss-PdbViewer[42], and polar hydrogens were added. The ES9 ligand was drawn three-dimensionally with Avogadro 1.1.1 (ref. 43) and was minimized with the built-in MMFF94s force field[44]. The AutoDockTools 1.5.4 suite[43] was used for pdbqt-format preparations of proteins and ligands. Dockings were with AutoDock-Vina 1.1.0 (ref. 45) with exhaustiveness set at 64; residues Arg64, Phe91 and Gln89 were set as flexible. The grid-box size was x = 20, y = 22 and z = 20 Å, centered at x = 50.0, y = -10.2 and z = 24.5. PyMOL was used for visualization[46,47].

Cloning, expression and purification of human and *Arabidopsis* nTD CHC1. Human and *Arabidopsis* nTD CHC1 (residues 1-363 amino acids) were cloned into the pGEX vector and transformed into the competent *Escherichia coli* BL21 cells. Transformed cells were cultured in LB medium supplemented with carbenicillin (amount?) at 37°C and the expression was induced by the addition of 1 mM isopropyl-1-thio-D-galactopyranoside (IPTG). Cell cultures were kept for another 4 h at 37°C. Cells were harvested by centrifugation (value?), resuspended in a buffer containing 10 mM Tris-HCl, pH 8.3, 500 mM NaCl, 10% (w/v?) glycerol and 5 mM β-mercaptoethanol and lysed by sonication. The proteins were purified by affinity purification on AKTA^{TM}. GSTrap FF 1-ml columns were first equilibrated with buffer (10 mM sodium phosphate buffer, 150 mM NaCl, pH 7.5) and then 5 ml of the sample was loaded onto a GSTrap column. Columns were subsequently washed with binding buffer and the bound proteins were eluted with the elution buffer (10 mM sodium phosphate buffer, 150 mM NaCl, 10 mM reduced glutathione, pH 7.5) and collected in 1-ml aliquots. The GST tag was cleaved by overnight thrombin digest at 20° C, whereafter the sample was again applied to a GSTrap column to remove the cleaved GST as well as uncleaved proteins. The flowthrough was collected and further polished by size exclusion chromatography with a SD75 16/600 column. Protein concentration (A_{280}) was measured with a Nanodrop 1000 (Thermo Scientific) and stored in a −80°C freezer.

Differential scanning fluorimetry (DSF) assay. For the DSF assay, the Light cycler 480, Real-time PCR system (Roche) was used as described previously[48]. The purified nTD of human and *Arabidopsis* CHC1 was diluted in a buffer containing 100 mM Hepes, pH 7.5, 150 mM NaCl. Each well of a 96-well microplate contained a concentration of 1.6 µM protein 2 µl of freshly prepared 1000× diluted 5000X Sypro Orange (Invitrogen), 2.5 µl of compound and buffer up to a total volume of 25 µl. Proteins were incubated with the compound or DMSO (5%) for 30 min in the dark. Thermal scanning (10 to 95°C at 1.5°C/min) was done with a real-time PCR setup and the fluorescence intensity was measured every 10 sec. The the software Light cycler 480Sw 1.5.1 was utilized for curve fitting, melting temperature calculation and report generation on the raw FTS data.

Microscale Thermophoresis (MST). MST experiments were conducted on a monolith NT.115 system (Nanotemper technologies) as described[49]. The purified nTD of the *Arabidopsis* CHC was labeled with the NT-647-NHS dye (Monolith NT™). ES9 was serially diluted (2 mM-4.5 µM) in the MST buffer and mixed in 1a :1 ratio with 200 nM of the *Arabidopsis* nTD CHC1 to yield a final volume of 20 µL per dilution. After 30 min of incubation at room temperature in the dark, the reaction mixture was loaded into standard treated capillaries and subsequently analyzed by MST at medium MST power (20%) and 50% LED power. Data were analyzed with the NT Affinity Analysis software. The normalized fluorescence (Fnorm) defined as the ratio of fluorescence level during the T jump (Fhot) to the baseline fluorescence (Fcold) were plotted against the ligand concentration in a concentration–response curve to provide an estimate of the Kd value upon fitting the data into the Kd model.

Transferrin uptake in HeLa cell cultures. HeLa cells were grown in DMEM (Gibco, Life technologies) containing 10% (w/v?) fetal calf serum (Gibco, Life Technologies) and 1% (w/v?) antibiotics (penicillin and/or? streptomycin) (Gibco, Life Technologies) in a

humidified incubator at 37°C under a 5% CO_2 atmosphere. All tested compounds were dissolved in DMSO and were diluted to the desired concentration in the DMEM medium without fetal calf serum and without phenol red (Gibco, Life technologies). Cells were pretreated with the compounds for 30 min followed by incubation with 25 µg/ml fluorescently labelled transferrin for 5-20 min. Imaging was done with a LSM 700 inverted confocal microscope (Zeiss) with a plan-apochromat 40×/1.2 water objective lens for a time period of up to 20 min after placement of the transferrin-containing cell solution. The images were quantified in ImageJ (Fiji) by measuring the signal intensities of the cells with mock treatment [between 0.01% (v/v) and 0.7% (v/v) DMSO] and of the compound-treated cells. For the WST-1 assay, HeLa cells were grown in a 96-well plate incubated with the compound for 30 min followed by addition of 10 µl WST-1 reagent to 100 µl of medium in a 96-well plate. Absorbance was measured at 450 nm versus a 650-nm reference by means of a plate reader.

Statistical tests and generation of graphs. All statistical tests and graphs other than boxplots were done and generated with a SigmaPlot 13. Boxplots were generated with the online tool BoxPlotR (http://boxplot.tyerslab.com/) from the Tyers and Rappsilber laboratories.

Life sciences reporting summary. **Further information on experimental design and reagents is available in the** Life Sciences Reporting Summary.

Data availability

References

40. Van Leene, J. *et al*. A tandem affinity purification-based technology platform to study the cell cycle interactome in *Arabidopsis thaliana*. *Mol. Cell. Proteomics* **6**, 1226-1238 (2007).

~~41. Van Gunsteren, W.F. *et al*. *Biomolecular simulation: the GROMOS96 manual and user guide*. vdf Hochschulverlag AG an der ETH Zürich, and BIOMOS b.v. Zürich, Groningen (1996).~~

41. Scott, W.R.P. *et al*. The GROMOS biomolecular simulation program package. *J. Phys. Chem. A* **103**, 3596-3607 (1999). Not better?

42. Guex, N. & Peitsch, M.C. SWISS-MODEL and the Swiss-Pdb Viewer: An environment for comparative protein modeling. *Electrophoresis* **18**, 2714–2723 (1997).

43. Hanwell, M.D. *et al*. Avogadro: an advanced semantic chemical editor, visualization, and analysis platform. *J. Cheminformatics* **4**, 17 (2012).

44. Halgren, T.A. MMFF VI. MMFF94s option for energy minimization studies. *J. Comput. Chem*. **20**, 720-729 (1999).

45. Trott, O. & Olson, A.J. AutoDock Vina: improving the speed and accuracy of docking with a new scoring function, efficient optimization and multithreading. *J. Comput. Chem*. **31**, 455-461 (2010).

46. Sanner, M.F. Python: a programming language for software integration and development. *J. Mol. Graph. Model*. **17**, 57-61 (1999).

47. DeLano, W.L. PyMOL: an open-source molecular graphics tool. Collaborative Computational Project no. 4 (CCP4) Newsletter On Protein Crystallography **40**, 82-92 (http://www.ccp4.ac.uk/newsletters/newsletter40/11_pymol.pdf).

DeLano, W.L (2009). The PyMOL Molecular Graphics System; DeLano Scientific: San Carlos, CA (2002). There is no corresponding record for this reference.

47. DeLano, W.L. *The PyMol Molecular Graphics System*. San Carlos, CA, DeLano Scientific (www.pymol.sourceforge.net/overview/sld001.htm) (2000). Not better?

48. Huynh, K. & Partch, C.L. Analysis of protein stability and ligand interactions by thermal shift assay.*Curr. Protoc. Protein Sci.* **79**, 28.9.1–28.9.14 (2015).

49. Jerabek-Willemsen, M. *et al*. MicroScale Thermophoresis: interaction analysis and beyond. *J. Mol. Struct*. **1077**, 101-113 (2014).

Figure legends

Figure 1 | ES9 binds clathrin heavy chain. Protein extracts from *Arabidopsis* PSB-D cell cultures were treated with ES9 (250 μM) or DMSO (Ø) for 30 min and the thermal denaturation curves for endogenous clathrin heavy chain (CHC) (**a**) and tubulin (**b**) were recorded across 12 temperature points (30-65°C). The relative band intensity compared to the ?? sample was measured by Western blot with anti-CHC and anti-tubulin antibodies. Error bars in (**a**) and (**b**) indicate SEM of three biological replicates. (**c**) Protein extracts from *Arabidopsis* PSB-D cell cultures were incubated with ES9 (250 μM) or DMSO (Ø) for 30 min and digested with different concentrations of pronase. An undigested sample was included as a control. The relative band intensity compared to the DMSO control was measured by Western blot with anti-CHC and anti-ATP synthase subunit β (ATPβ) antibodies. **P*<0.5, ***P*<0.01 relative to the control (Student's *t*-test) from three biological replicates (**d**) Changes in the thermodynamic stability of the *Arabidopsis* CHC1 N-terminal domain (nTD) in the presence of different concentrations of ES9 and the inactive analog ES9-6. The data shown are representative of three experiments. RFU, relative fluorescence units.

Figure 2 | ES9 binds the terminal domain of clathrin heavy chain. (**a**) The structure of the human clathrin heavy chain 1 (CHC1) N-terminal domain (nTD) (green cartoon) is shown in complex with ES9 (salmon) (**b**). Omitted electron density (2Fo − Fc) of ES9, contoured at 1σ level, is observed inside the hydrophobic clathrin box, which is located between the first and second blades of the nTD. (**c**) The interaction distances between the nTD residues and ES9 are shown with yellow dashes. The zoom-in view of the benzonitro moiety of ES9 indicates that the oxygen of the nitro group interacts electrostatically with R64. (**d**) A 60-degree rotated view of ES9 focuses on the bromothiophene moiety. Whereas the sulfur atom of the

thiophene group is shown in close contact to the carboxyl oxygen of S67, the bromide atom points toward the carboxyl oxygen of L82 by a σ hole.

Figure 3 | ES9-17 is not a protonophore. (**a**) Structure of ES9-17. (**b**) Dose-response of ES9-17-mediated FM4-64 uptake inhibition. The data are plotted as the ratio of the plasma membrane (PM) over the cytoplasmic FM4-64 fluorescence intensities. EC50 is 13 µM. (**c**) Strongly reduced FM4-64 uptake (2 µM, 30 min) in *Arabidopsis* root epidermal cells in the presence of ES9-17 (30 µM) when compared to the DMSO (Ø) control. The samples were pretreated with either ES9-17 (30 µM) or DMSO for 30 min. (**d**) Measurements of the ATP concentration in dark-grown wild type *Arabidopsis* PSB-D cell cultures treated for 30 min with ES9 (10 µM), ES9-17 (30 µM) and ES9-6 (50 µM), showing the ATP concentration relative to the DMSO control. Error bars indicate SEM of three biological replicates. (**e**) Confocal images of *Arabidopsis* epidermal root cells stained with Lyso Tracker Red DND 99 (30 min) and treated additionally for 30 min with DMSO (Ø), ES9 (10 µM) or ES9-17 (30 µM). Scale bars, 10 µm.

Figure 4 | ES9-17 is a CME inhibitor. (**a**) ES9-17 inhibited the recruitment of the plasma membrane-localized BRI1 to the Brefeldin A (BFA) body. Samples were pretreated with 50 µM cycloheximide (CHX) for 1 h and treated with either DMSO (Ø) or ES9-17 (30 µM) for 30 min, followed by a combined application of FM4-64 (2 µM) and BFA (50 µM) for an additional 30 min in the presence of the inhibitor. Scale bars, 10 µm. (**b**) Confocal images *of Arabidopsis* root epidermal cells expressing PEPR1-GFP. Seedlings were treated with ES9-17 (30 µM) or DMSO (Ø) for 30 min, followed by elicitation with 100 nM Pep1. The internalization of the Green Fluorescent Protein (GFP)-tagged PEPR1 was followed until 90 min post elicitation. Scale bars, X µm. (**c**) Boxplot representation of the transferrin uptake

in HeLa cells in the presence of ES9-17 (30 μM) and DMSO (Ø) from 5 to 20 min. Center lines show the medians; box limits indicate the 25th and 75th percentiles as determined by R software; outliers are represented by dots. (**d**) Histograms representing the measured endocytic foci life time of CLC1-GFP in the presence of ES9-17 (30 μM) or DMSO (Ø), n=X? and X? measurements, respectively. Kymographs represent a line trace (horizontal axis) over a time period (vertical axis), taken from a time lapse (2 f/sec) of *Arabidopsis* root epidermal cells, that illustrates the life times of endocytic foci labeled by CHC1-GFP. Scale bar, 10 sec.

Figure 5 |ES9-17 targets clathrin heavy chain. Protein extracts from *Arabidopsis* PSB-D cell cultures were treated with ES9-17 (250 μM) or DMSO (Ø) for 30 min. The thermal denaturation curves for endogenous clathrin heavy chain (CHC) (**a**) and tubulin (**b**) were observed across 12 temperature points (30-65°C). The relative band intensity compared to the ?? sample was measured by Western blot using anti-CHC and anti-tubulin antibodies. Error bars in (**a**) and (**b**) indicate SEM of three biological replicates. (**c**) Protein extracts from *Arabidopsis* PSB-D cell cultures were incubated with ES9-17 (250 μM) or DMSO (Ø) for 30 min and digested with different concentrations of pronase. An undigested sample was included as a control. The relative band intensity compared to the DMSO control was measured by Western blot with anti-CHC and anti-ATP synthase subunit β (ATPβ) antibodies. **P*<0.5, ***P*<0.01 relative to the control (Student's *t*-test) from three biological replicates. (**d**) Boxplot representation of the root growth fold change over 48 h for wild type *Arabidopsis* Col-0 seedlings treated with ES9-17 (12 μM). Center lines show the medians; box limits indicate the 25th and 75th percentiles as determined by the R software, outliers are represented by dots. n=80, **P*<0.05, ****P*<0.001 one-way analysis of variance (ANOVA) test.

Supplementary Fig. 1 | Structure activity relation (SAR) analysis of ES9 for the attachment of the linker-biotin group. (**a**) Chemical structures of ES9 analogs as part of the SAR analysis to establish a suitable appending position for a linker-biotin group. (**b**) FM4-64 uptake assay. *Arabidopsis* wild type Col-0 seedlings were cotreated with the small molecules at a concentration of 50 μM and FM4-64 (2 μM) for 30 min after pretreatment with the inhibitors for 30 min. Scale bar, 10 μm.

Supplementary Fig. 2 | ES9 binds *Arabidopsis* and human clathrin heavy chain (CHC). (**a**) Protein extracts from *Arabidopsis* PSB-D cell cultures were treated with increasing concentrations of ES9 for 30 min to obtain dose-response curves for endogenous clathrin heavy chain (CHC) and ATP synthase subunit β (ATPβ) at 46°C. The relative band intensity as compared to the DMSO sample was measured by Western blot with anti-CHC and anti-ATPβ antibodies. (**b**) Protein extracts from *Arabidopsis* PSB-D cell cultures were treated with ES9 (250 μM) or DMSO (Ø) for 30 min. The thermal denaturation curve for the endogenous ATPβ was determined. The relative band intensity as compared to the X sample was measured by Western blot with anti-ATPβ antibodies. (**c**) Protein extracts from *Arabidopsis* PSB-D cell cultures were treated with the inactive ES9-6 analog (250 μM) or DMSO (Ø) for 30 min. The thermal denaturation curves for endogenous CHC was determined. The relative band intensity as compared to the X sample was measured by Western blot with anti-CHC antibodies. Error bars (**a-c**) indicate SEM of three biological replicates. (**d**) Changes in the thermodynamic stability of the human N-terminal domain (nTD) of CHC1 in the presence of increasing concentrations of ES9 and its inactive analog ES9-6. The data are shown as representative of three experiments.

Supplementary Fig. 3 | Molecular docking of ES9 with human clathrin heavy chain (CHC) N-terminal domain (nTD). (**a**) (left) Best-docked position of ES9 (sticks, white carbons) in human CHC N-terminal domain (nTD) pdb-entry 4G55. Zoom into the recognition site of Pitstop2 (lines, orange). The residues Arg64 (top left), Phe91 (bottom center) and Gln89 (bottom right) that had been set as flexible during docking are shown as green sticks. This docked position is very similar to that of ES9 in the later obtained ES9-complexed CHC nTD crystal structure. (right) Best-docked position of ES9-17 (sticks, white carbons) in human CHC N-terminal domain (nTD) pdb-entry 4G55. Zoom into the recognition site of Pitstop2 (lines, orange). The residues Arg64 (top left), Phe91 (bottom center) and Gln89 (bottom right) that had been set as flexible during docking are shown as green sticks. This docked position is very similar to that of the ES9 docking in the CHC nTD. (**b**) Amino acid sequence alignment of the nTD domains of *Arabidopsis* CHC1 and CHC2 and the human CHC1. The CLC workbench was used for the alignment. Different types of amino acids are color coded. The consensus sequence is depicted below the alignment. Pink highlights indicate the amino acids predicted to be part of the binding pocket, according to I-TASSER.

Supplementary Fig. 4 | Structure activity relation (SAR) analysis of ES9 to identify nonprotonophoric analogs. (**a**) SAR analysis of ES9 to identify an analog lacking the protonophore activity. (**b**) *Arabidopsis* wild type Col-0 seedlings were cotreated with the small molecules at a concentration of 50 µM and FM4-64 (2 µM) for 30 min after pretreatment with the inhibitors for 30 min. Scale bar, 10 µm. (**c**) *Arabidopsis* Col-0 seedlings were treated with the small molecules (50 µM, 30 min) followed by a treatment with MitoTracker Red CM-H2xRos (250 nM) for another 30 min. Scale bar, ?

Supplementary Fig. 5 | ES9-17 does not inhibit organelle and cytoskeleton motility. (**a**) Fluorescein diacetate (FDA) measurements in dark-grown wild type *Arabidopsis* PSB-D cell cultures treated for 30 min with ES9 (10 µM), ES9-17 (30 µM), ES9-6 (50 µM) and DMSO (Ø). Error bars indicate SE of the mean (SEM) of three biological replicates (**b**) TGN (VHA-a1-GFP) and (**c**) Golgi (ST-mRFP) after 30 min incubation in the presence of DMSO (Ø), ES9 (10 µM) and ES9-17 (30 µM). (**d**) The actin cytoskeleton, labeled by Fimbrin-GFP and (**e**) the microtubules, labeled by MAP4-GFP were not affected by ES9-17. All seedlings were pretreated for 30 min with DMSO (Ø), ES9 (10 µM) and ES9-17 (30 µM). Images (**b-d**) are composed of six differentially colored images taken over 90 sec with an interval of 10 sec. Scale bars (**b-d**), ?

Supplementary Fig. 6 | ES9-17 is an inhibitor of clathrin-mediated endocytosis (CME) in *Arabidopsis* and HeLa cells. (**a**) BFA compartments were formed in the presence of ES9-17. Seedlings expressing the TGN/EE marker VHA-a1-GFP were treated with 50 µM CHX for 1 h and either with DMSO (Ø) or ES9-17 (30 µM) for 30 min, followed by FM4-64 (2 µM) and BFA (50 µM) for an additional 30 min in the presence of either DMSO or the inhibitor. (**b**) Confocal images of *Arabidopsis* seedlings expressing BRI1-GFP treated with DMSO (Ø) or ES9-17 (30 µM) for 30 min followed by a treatment with Alexa Fluor 647-castasterone (AFCS) for 10 min followed by a chase of 20 min. Scale bars (**a** and **b**), 10 µm. (**c**) Boxplot representation of the transferrin uptake in HeLa cells in the presence of DMSO (Ø) and Pitstop2 (20 µM) from 5 to 20 min. Center lines show the medians; box limits indicate the 25th and 75th percentiles as determined by the R software, outliers are represented by dots. (**d**) Quantification of the formazan dye, produced by metabolically active Hela cells upon treatment with ES9-17, Pitstop2 and DMSO (Ø) (as described **Fig. 4c)** and the WST-1 cell proliferation assay. (**e**) Histograms representing the measured endocytic foci life-time of GFP-

tagged CHC1 and TPLATE muniscin-like (TML) (Ø). n=1393 and 520 measurements (CHC1-GFP), n=2389 and 287 measurements (TML-GFP) in the presence of ES9-17 (30 µM) or DMSO, respectively. Kymographs representing a line trace (horizontal axis) over a time period (vertical axis), taken from a time-lapse (2 f/sec) of *Arabidopsis* root epidermal cells, and illustrating the life times of endocytic foci labeled by the TML-GFP. Scale bar, 10 sec.

Supplementary Fig. 7 | ES9-17 targets clathrin heavy chain (CHC). (**a**) *Arabidopsis* cell lysate was treated with increasing concentrations of ES9-17 to obtain dose-response curves for CHC and ATPβ at a fixed temperature (46°C). (**b**) *Arabidopsis* cell lysate was treated with ES9-17 (250 µM) or mock (Ø, DMSO) for 30 min. Thermal denaturation for endogenous ATPβ was observed by Western blots. (**a**, **b**) Quantification was made by measuring the band intensity on the Western blot relative to DMSO. Error bars indicate SEM of three biological replicates **(c)** Root growth of *Arabidopsis* seedlings treated with increasing concentrations of ES9-17 growing on ½MS media supplemented with 100 mM sucrose. EC50 = 9 µM. **(d)** Boxplot representation of the root growth fold change over 48 h of *Arabidopsis* Col-0 seedlings and the *chc1-3*, *chc2-1* and *chc2-2* mutant alleles on ½MS media supplemented with 100 mM sucrose and DMSO (Ø). n=80; n. s., nonsignificant for a one-way analysis of variance (ANOVA) test. **(e-g**) *Arabidopsis* cell lysate was incubated with ES9-17 (250 µM) or DMSO (Ø) and digested with different concentrations of pronase. An undigested sample was included as control. Quantification was made by measuring the band intensity on Western blots relative to DMSO. Error bars indicate SEM.

Supplementary Table 1. List of identified proteins for the ES9-10 and ES9-13 affinity purification. Numbers indicate the times a protein is found out of nine repeats (three biological repeats, each consisting of three technical repeats).

Supplementary Table 2. Thermal stability of the N-terminal domain (nTD) of clathrin heavy chain1 (CHC1) of *Arabidopsis thaliana* (At) and *Homo sapiens* (Hs) in the presence of various concentrations of ES9.

Supplementary Table 3. Data collection and refinement statistics

Supplementary Table 4. Primers used in this study

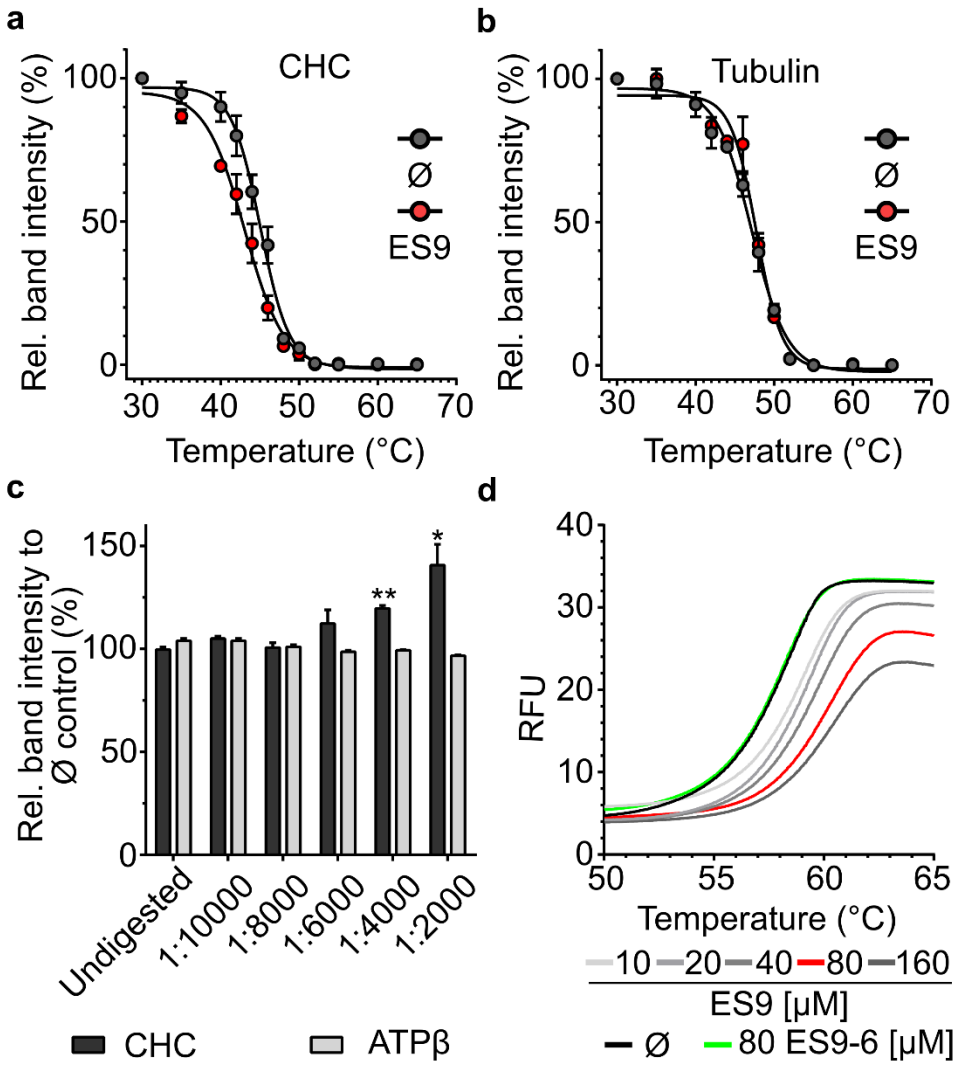
a
CHC
Rel. band intensity (%)
100
50
0
30
40
50
60
70
Temperature (°C)
Ø
ES9
b
Tubulin
Rel. band intensity (%)
100
50
0
30
40
50
60
70
Temperature (°C)
Ø
ES9
c
Rel. band intensity to Ø control (%)
150
100
50
0
**
*
Undigested
1:10000
1:8000
1:6000
1:4000
1:2000
CHC
ATPβ
d
RFU
40
30
20
10
0
50
55
60
65
Temperature (°C)
10
20
40
80
160
ES9 [µM]
Ø
80 ES9-6 [µM]

Figure 1

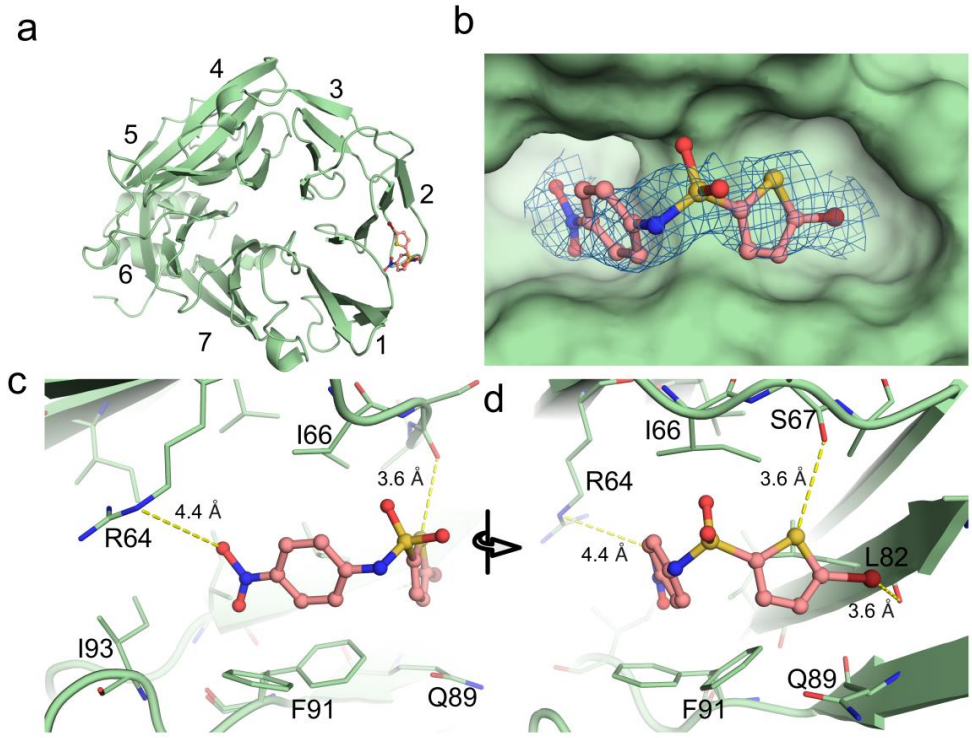
a
b
4
3
5
2
6
7
1
c
d
I66
3.6 Å
4.4 Å
R64
I93
F91
Q89
I66
S67
R64
3.6 Å
4.4 Å
L82
3.6 Å
Q89
F91

Figure 2

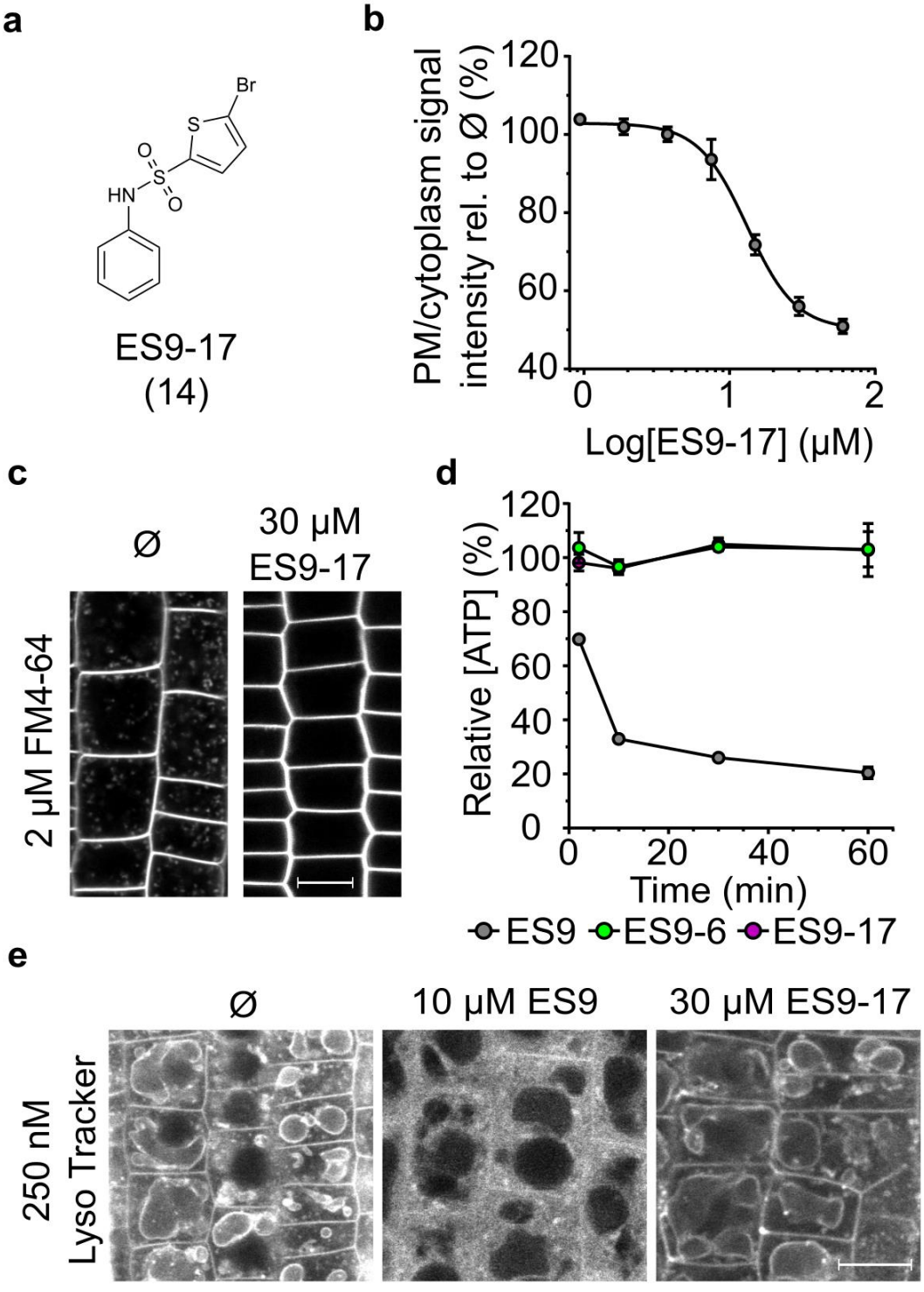
a
Br
S
O
S
O
HN
ES9-17
(14)
b
PM/cytoplasm signal
intensity rel. to Ø (%)
120
100
80
60
40
0
1
2
Log[ES9-17] (µM)
c
Ø
30 µM
ES9-17
2 µM FM4-64
d
Relative [ATP] (%)
120
100
80
60
40
20
0
0
20
40
60
Time (min)
ES9
ES9-6
ES9-17
e
Ø
10 µM ES9
30 µM ES9-17
250 nM
Lyso Tracker

Figure 3

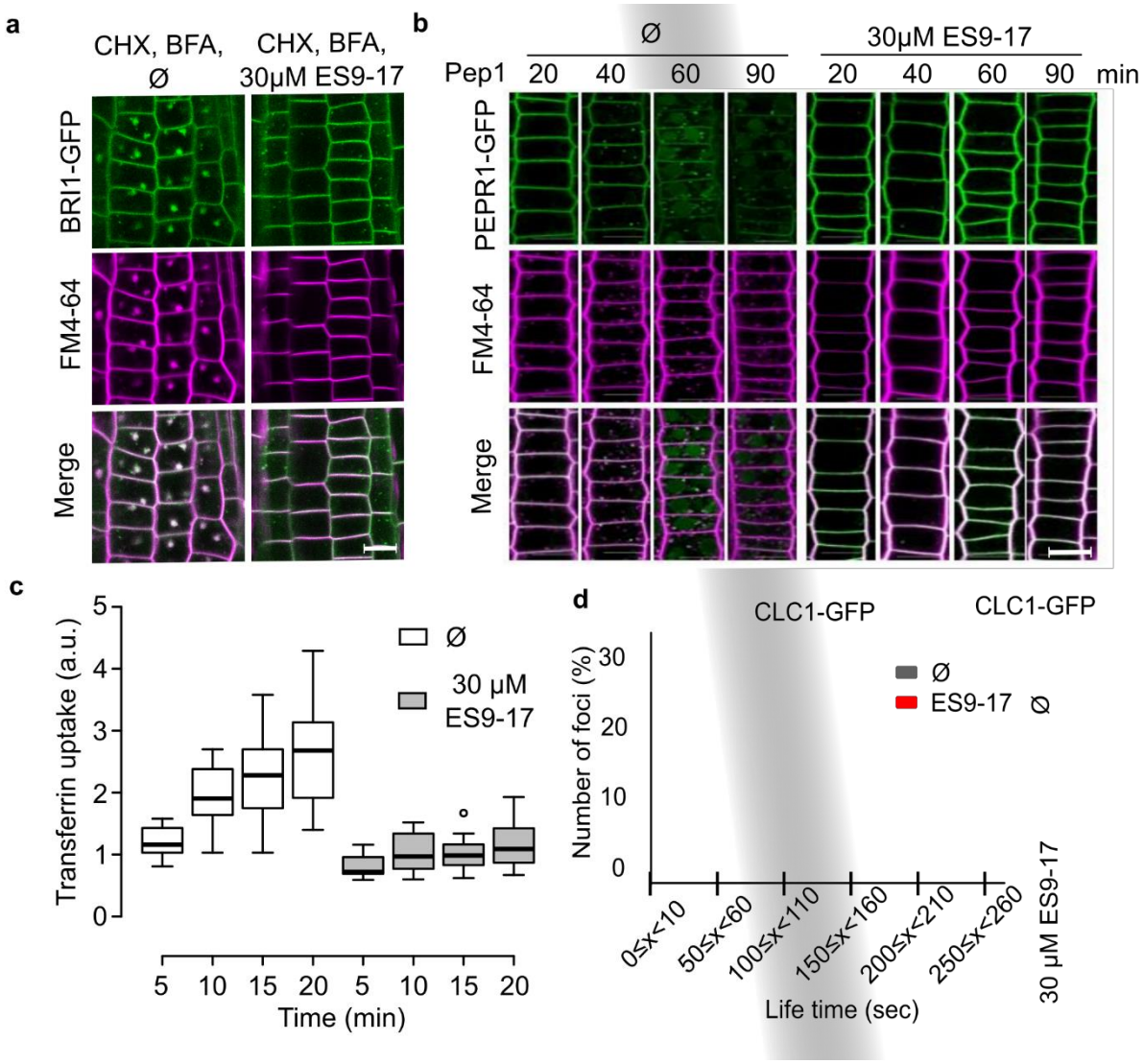
a
CHX, BFA, Ø
CHX, BFA, 30μM ES9-17
BRI1-GFP
FM4-64
Merge
b
Ø
30μM ES9-17
Pep1
20 40 60 90 20 40 60 90 min
PEPR1-GFP
FM4-64
Merge
c
Transferrin uptake (a.u.)
Ø
30 μM ES9-17
Time (min)
d
CLC1-GFP
CLC1-GFP
Number of foci (%)
Ø
ES9-17
Ø
0≤x<10
50≤x<60
100≤x<110
150≤x<160
200≤x<210
250≤x<260
Life time (sec)
30 μM ES9-17

Figure 4

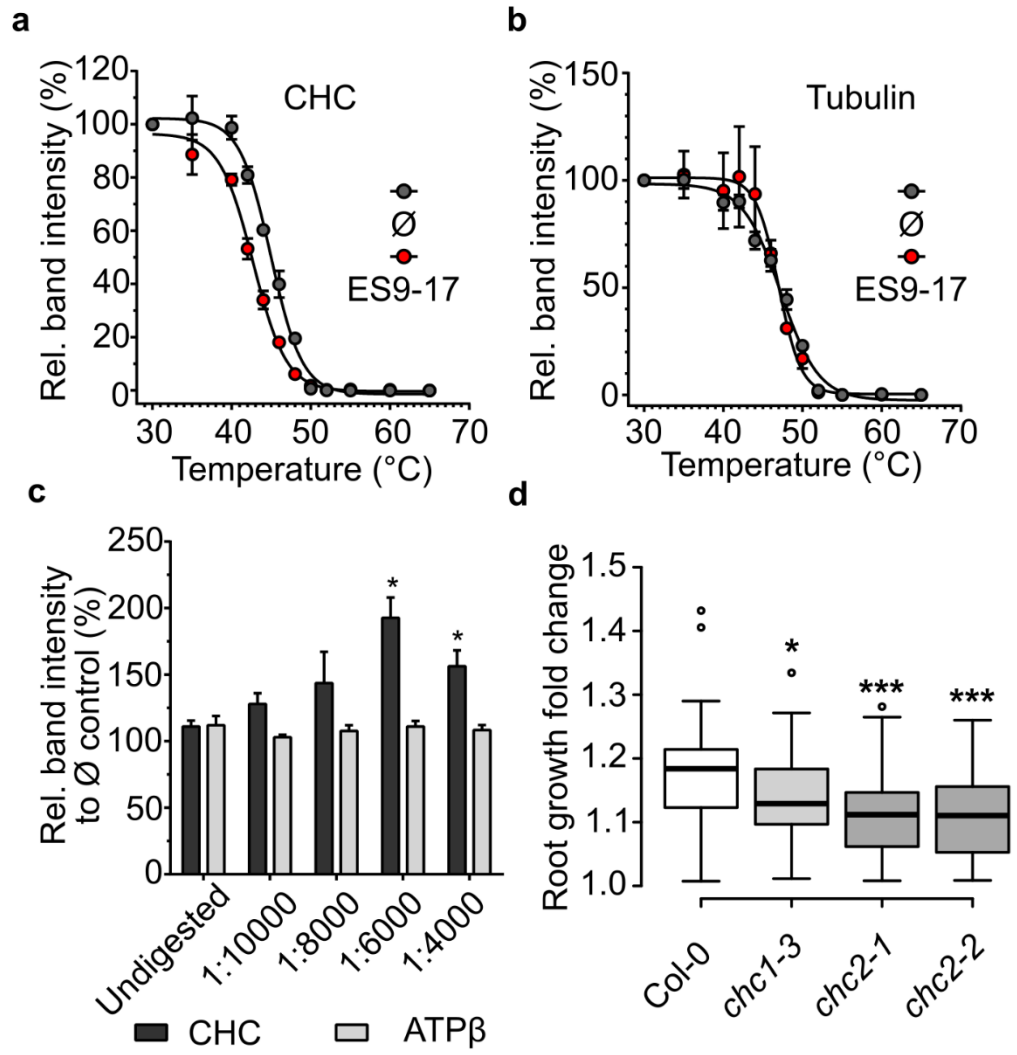
a
b
CHC
Tubulin
Rel. band intensity (%)
Temperature (°C)
Ø
ES9-17
c
d
Rel. band intensity to Ø control (%)
Undigested
1:10000
1:8000
1:6000
1:4000
CHC
ATPβ
Root growth fold change
Col-0
chc1-3
chc2-1
chc2-2

Figure 5

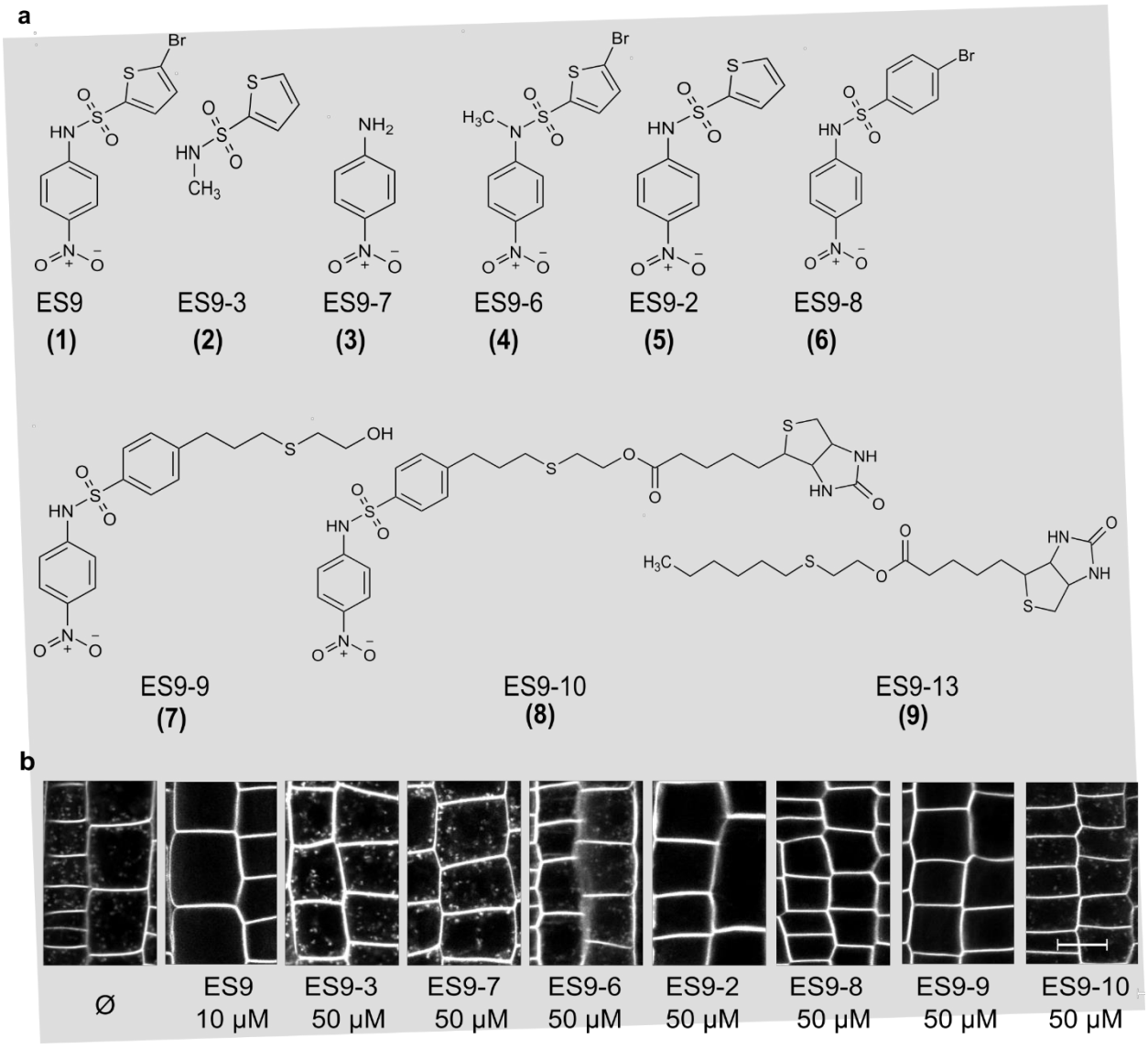

Supplementary Fig. 1

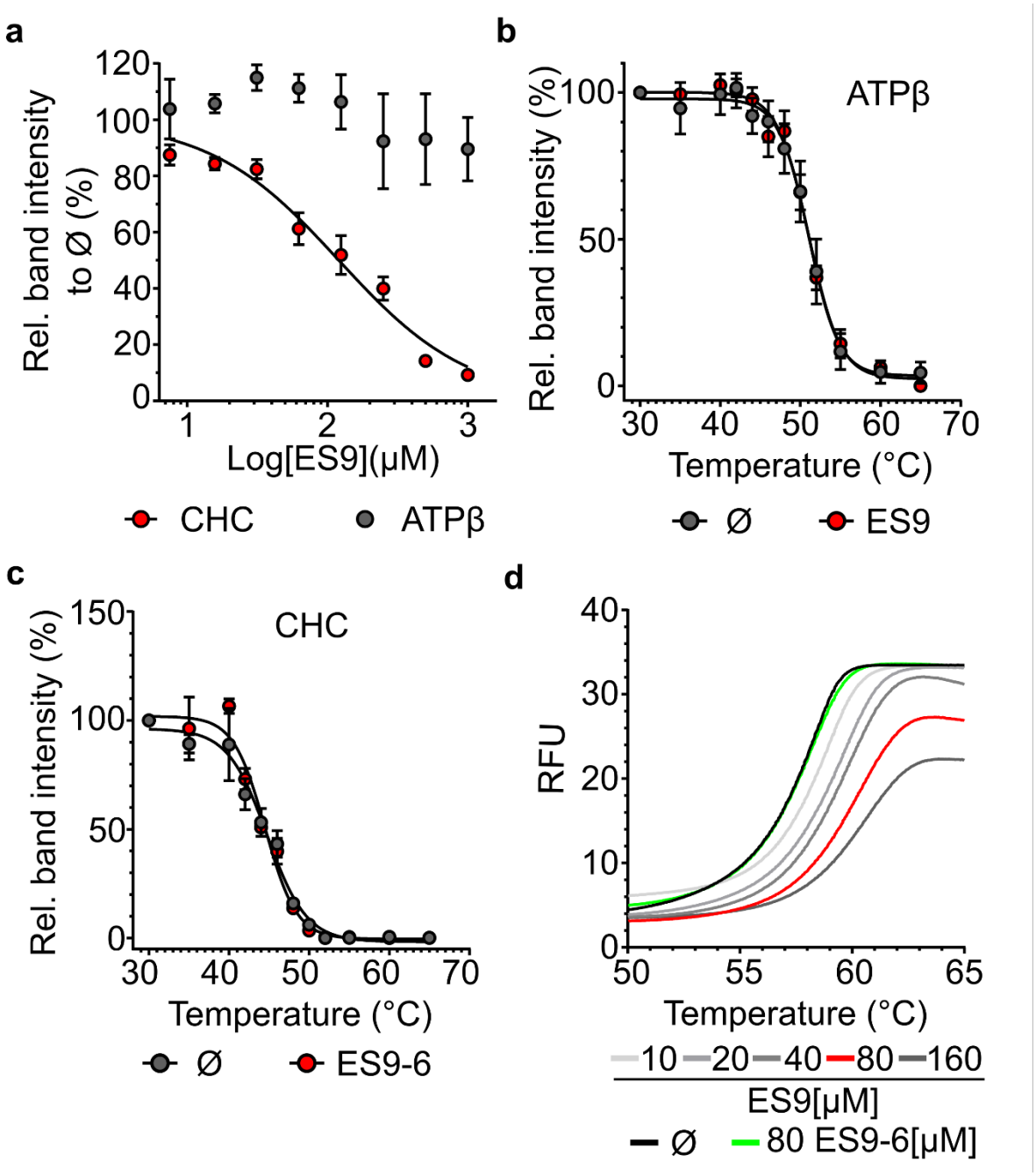

Supplementary Fig. 2

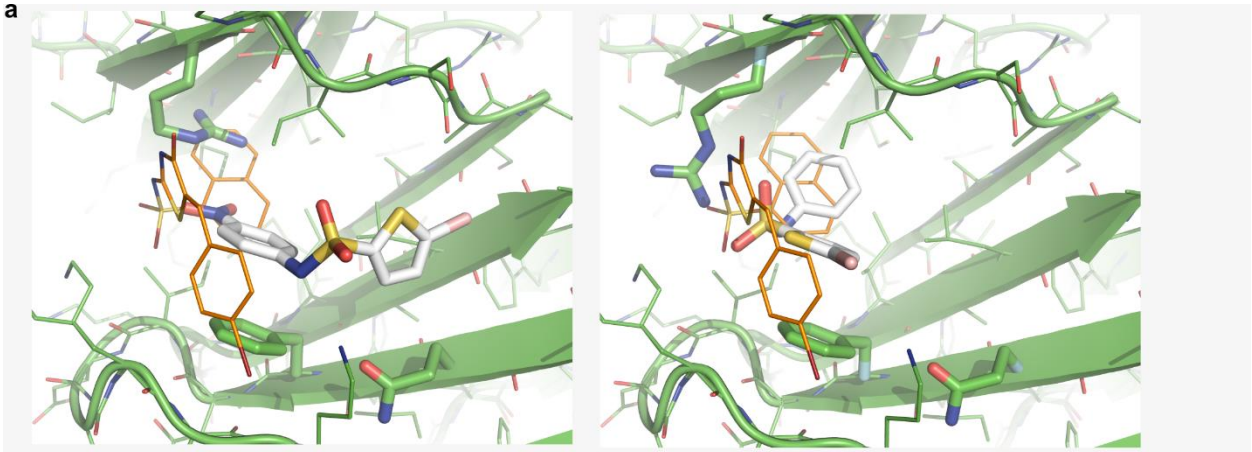

b

```
AtCHC1 nTD  MAAANAPIIM KEVLTLPSVG IGQQFITFTN VTMESDKYIC VRE-TAPQNS VVIIDMNMPM QPLRRPITAD SALMNPNSRI 79
AtCHC2 nTD  MAAANAPITM KEVLTLPSIG INQQFITFTN VTMESDKYIC VRE-TSPQNS VVIIDMNMPM QPLRRPITAD SALMNPNSKI 79
HsCHC1 nTD  MAQI-LPIRF QEHLQLQNLG INPANIGFST LTMESDKFIC IREKVGEQAQ VVIIDMNDPS NPIRRPISAD SAIMNPASKV 79
Consensus   MAAANAPI*M KEVLTLPS*G INQQFITFTN VTMESDKYIC VRE-T*PQNS VVIIDMNMPM QPLRRPITAD SALMNPNSKI

AtCHC1 nTD  LALKAQVPGT TQDHLQIFNI EAKAKLKSHQ MPEQVAFWKW ITPKMLGLVT QTSVYHWSIE GDSEPVKMFD RTANLANNQI 159
AtCHC2 nTD  LALKAQVPGT TQDHLQIFNI EAKAKLKSHQ MPEQVVFWKW ITPKMLGLVT QNSVYHWSIE GDSEPVKMFD RTANLANNQI 159
HsCHC1 nTD  IALKA---GK T---LQIFNI EMKSKMKAHT MTDDVTFWKW ISLNTVALVT DNAVYHWSME GESQPVKMFD RHSSLAGCQI 153
Consensus   LALKAQVPGT TQDHLQIFNI EAKAKLKSHQ MPEQV*FWKW ITPKMLGLVT QNSVYHWSIE GDSEPVKMFD RTANLANNQI

AtCHC1 nTD  INYKCSPNEK WLVLIGIAPG SPERPQLVKG NMQLFSVDQQ RSQALEAHAA SFAQFKVPGN ENPSILISFA SKSFNAGQIT 239
AtCHC2 nTD  INYKCSPNEK WLVLIGIAPG SPERQQLVKG NMQLFSVDQQ RSQALEAHAA SFAQFKVPGN ENPSILISFA SKSFNAGQIT 239
HsCHC1 nTD  INYRTDAKQK WLLLTGISA- ---QQNRVVG AMQLYSVDRK VSQPIEGHAA SFAQFKMEGN AEESTLFCFA VR----GQAG 225
Consensus   INYKCSPNEK WLVLIGIAPG SPERQQLVKG NMQLFSVDQQ RSQALEAHAA SFAQFKVPGN ENPSILISFA SKSFNAGQIT

AtCHC1 nTD  SKLHVIELGA QP-GKPSFTK KQADLFFPPD FADDFPVAMQ VSHKFNLIYV ITKLGLLFVY DLETASAIYR NRISPDPIFL 318
AtCHC2 nTD  SKLHVIELGA QP-GKPSFTK KQADLFFPPD FADDFPVAMQ VSHKFNLIYV ITKLGLLFVY DLETASAIYR NRISPDPIFL 318
HsCHC1 nTD  GKLHIIEVGT PPTGNQPFPK KAVDVFFPPE AQNDFPVAMQ ISEKHDVVFL ITKYGYIHLY DLETGTCIYM NRISGETIFV 305
Consensus   SKLHVIELGA QP-GKPSFTK KQADLFFPPD FADDFPVAMQ VSHKFNLIYV ITKLGLLFVY DLETASAIYR NRISPDPIFL

AtCHC1 nTD  TSEASSVGGF YAINRRGQVL LATVNEATII PFISGQLNNL ELAVN----- -------- 363
AtCHC2 nTD  TSEASSVGGF YAINRRGQVL LATVNEATII PFISGQLNNL ELAVN----- -------- 363
HsCHC1 nTD  TAPHEATAGI IGVNRKGQVL SVCVEEENII PYITNVLQNP DLALRMAVRN NLAGAEEL 363
Consensus   TSEASSVGGF YAINRRGQVL LATVNEATII PFISGQLNNL ELAVN----- --------
```

Supplementary Fig. 3

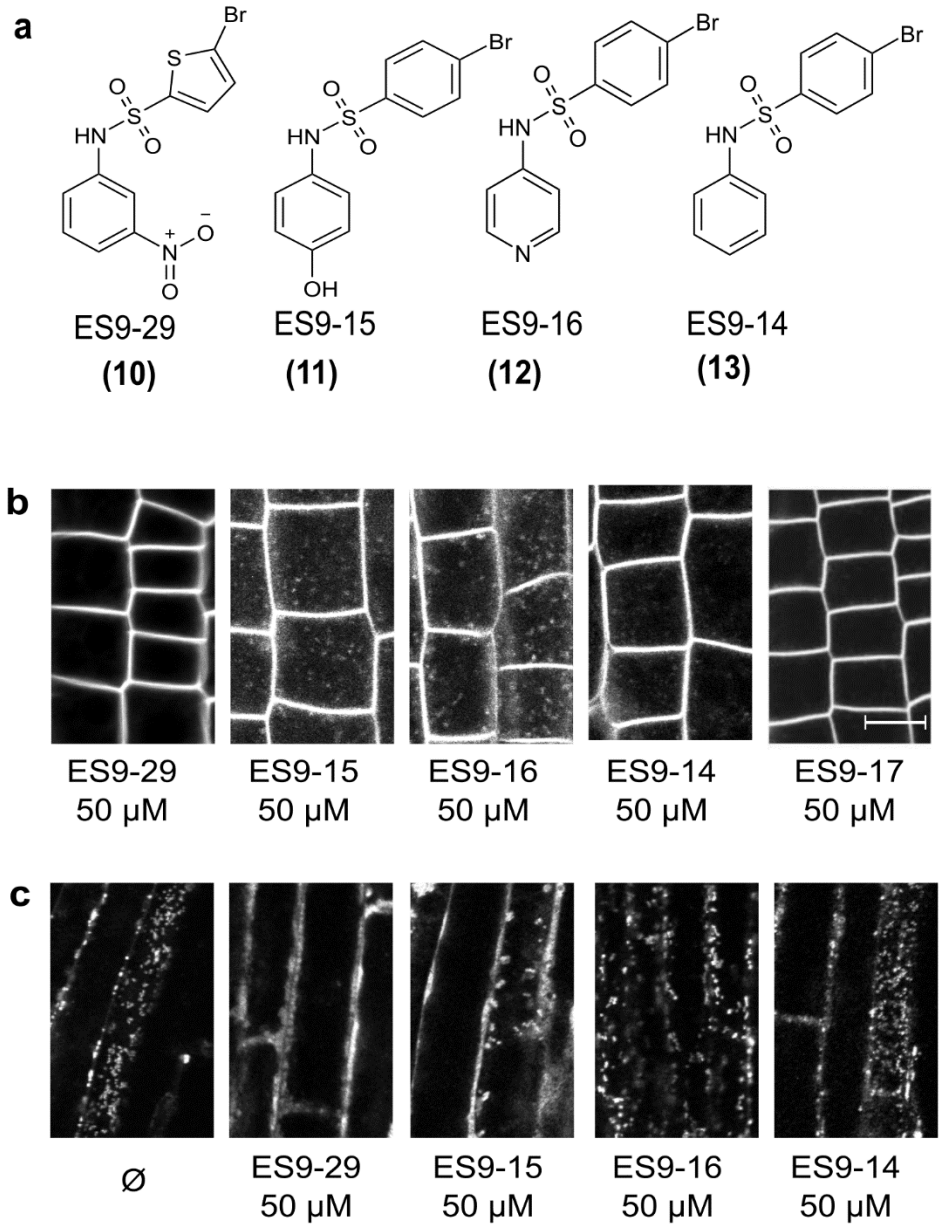

Supplementary Fig.4

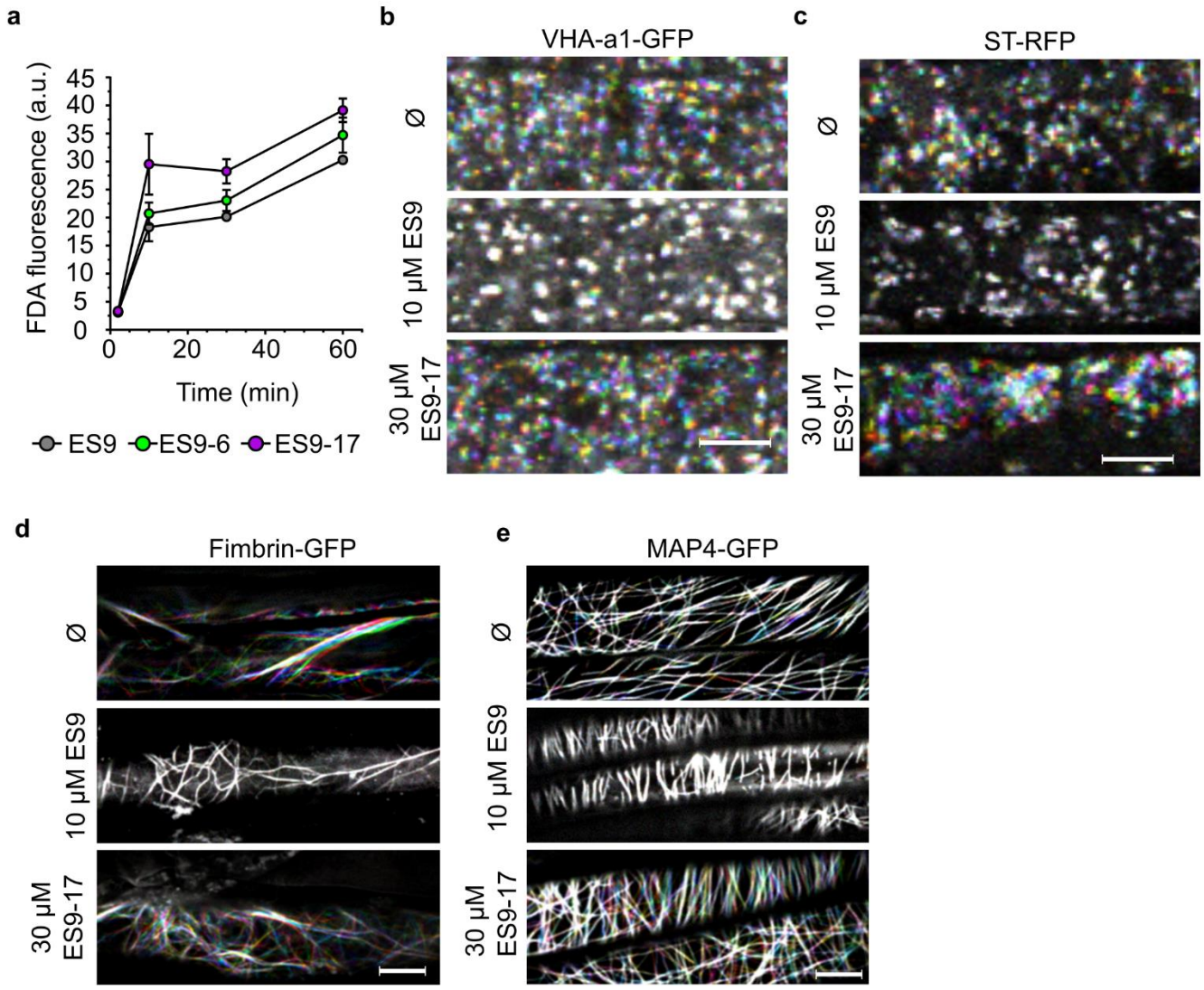

Supplementary Fig. 5

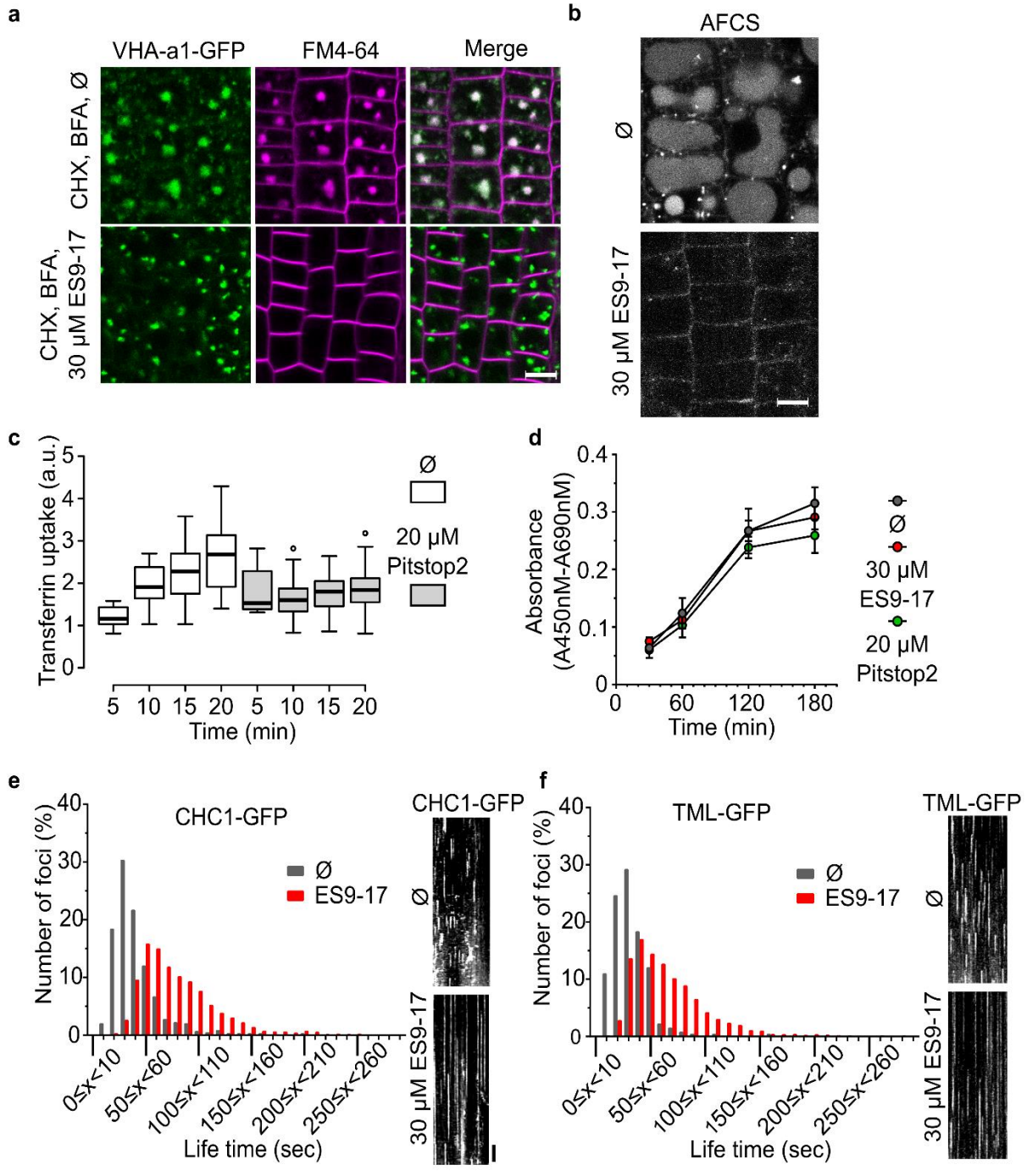

Supplementary Fig. 6

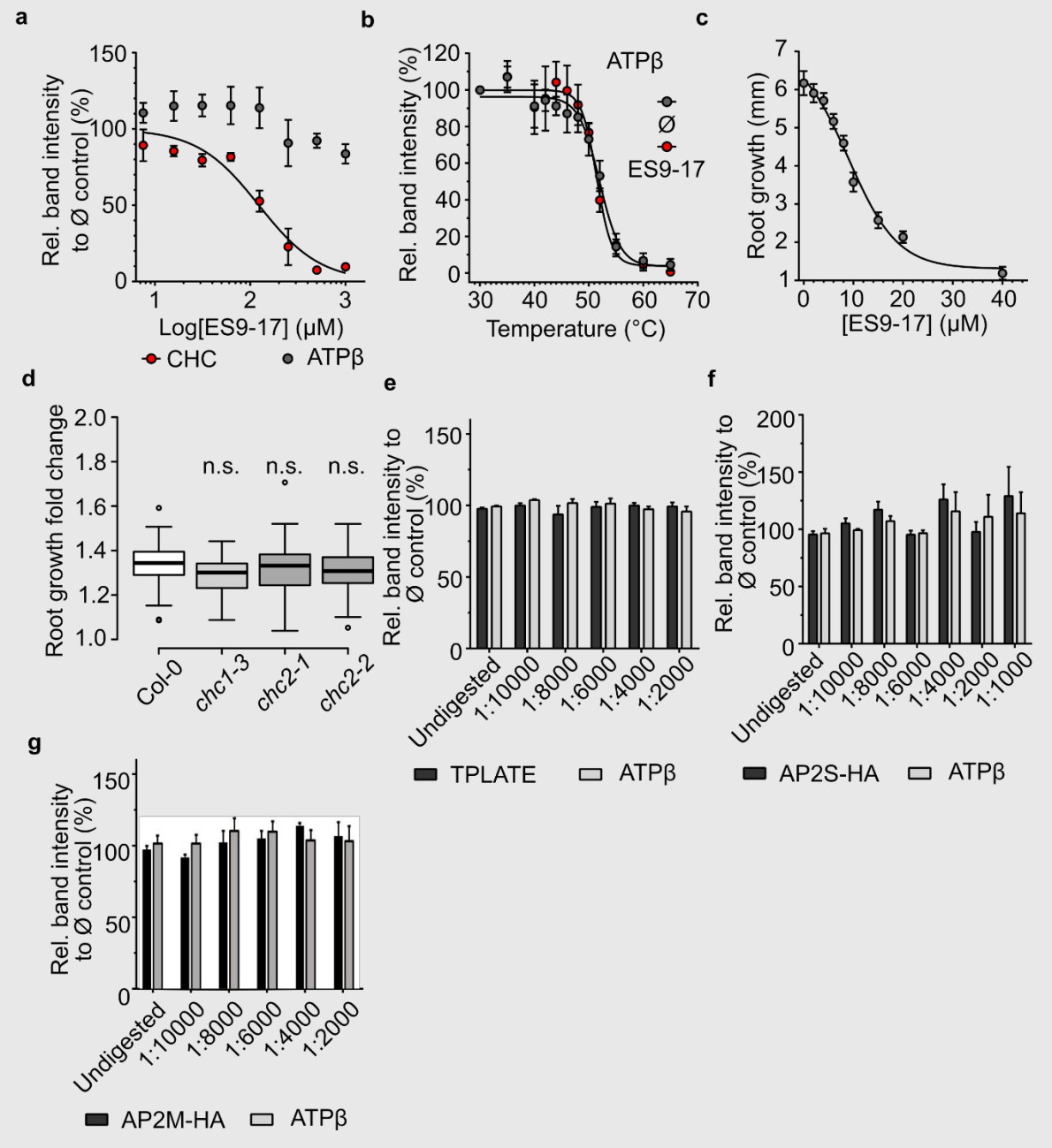

Supplementary Fig. 7